Contrib Mineral Petrol (2003) 145: 228–250
DOI 10.1007/s00410-003-0446-1

ORIGINAL PAPER

Boswell A. Wing · John M. Ferry · T. Mark Harrison

Prograde destruction and formation of monazite and allanite during contact and regional metamorphism of pelites: petrology and geochronology

Received: 19 February 2002 / Accepted: 17 December 2002 / Published online: 29 March 2003

Abstract The conditions at which monazite and allanite were produced and destroyed during prograde metamorphism of pelitic rocks were determined in a Buchan and a Barrovian regional terrain and in a contact aureole, all from northern New England, USA. Pelites from the chlorite zone of each area contain monazite that has an inclusion-free core surrounded by a highly irregular, inclusion-rich rim. Textures and $^{208}Pb/^{232}Th$ dates of these monazites in the Buchan terrain, obtained by ion microprobe, suggest that they are composite grains with detrital cores and very low-grade metamorphic overgrowths. At exactly the biotite isograd in the regional terrains, composite monazite disappears from most rocks and is replaced by euhedral metamorphic allanite. At precisely the andalusite or kyanite isograd in all three areas, allanite, in turn, disappears from most rocks and is replaced by subhedral, chemically unzoned monazite neoblasts. Allanite failed to develop at the biotite isograd in pelites with lower than normal Ca and/or Al contents, and composite monazite survived at higher grades in these rocks with modified texture, chemical composition, and Th–Pb age. Pelites with elevated Ca and/or Al contents retained allanite in the andalusite or kyanite zone. The best estimate of the time of peak metamorphism at the andalusite or kyanite isograd is the mean Th–Pb age of metamorphic monazite neoblasts that have not been affected by retrograde metamorphism: 364.3 ± 3.5 Ma in the Buchan terrain, 352.9 ± 8.9 Ma in the Barrovian terrain, and 403.4 ± 5.9 Ma in the contact aureole. Some metamorphic monazites from the Buchan terrain have ages partially to completely reset during an episode of retrograde metamorphism at 343.1 ± 9.1 Ma. Interpretation of Th–Pb ages of individual composite monazite grains is complicated by the occurrence of subgrain domains of detrital material intergrown with domains of material formed or recrystallized during prograde and retrograde metamorphism.

B.A. Wing (✉)
Department of Earth and Planetary Sciences,
Johns Hopkins University, Baltimore, MD , 21218, USA
E-mail: wing@essic.umd.edu
Tel.: +1-301-4052149
Fax: +1-301-4059661

J.M. Ferry
Department of Earth and Planetary Sciences,
Johns Hopkins University, Baltimore, MD , 21218, USA

T.M. Harrison
Research School of Earth Sciences, The Australian National University, Mills Road, ACT 0200 Canberra, Australia

Present address: B.A. Wing
Earth System Science Interdisciplinary Center, University of Maryland, College Park, MD , 20742, USA

Editorial responsibility: T.L. Grove

Introduction

Monazite, approximately $(LREE,Th)PO_4$, is a ubiquitous trace mineral in suites of metamorphosed pelitic rocks (Overstreet 1967). Because monazite can develop as a prograde metamorphic mineral and because of its relatively large Th and U contents (Parrish 1990), much effort has been devoted over the last decade to development of methods for dating the mineral, including thermal ionization mass spectrometry, ion microprobe analysis, and electron microprobe analysis (Harrison et al. 2002). As voiced by many, however (e.g., Pan 1997; Finger et al. 1998; Vance et al. 1998; Foster et al. 2000; Simpson et al. 2000; Hildebrand et al. 2001; Pyle et al. 2001), the ability to interpret radiometric ages of monazite in metamorphic rocks has not kept pace with the technical ability to obtain those dates because the reactions by and conditions at which monazite develops during prograde metamorphism are not well understood. Much of the uncertainty in the behavior of monazite during metamorphism has resulted from attempts to draw general conclusions from studies that involved relatively small sample sets, incomplete coverage of all metamorphic zones, and a variety of rock

types. This investigation resolved some of the questions about the reactions and conditions at which monazite forms during metamorphism by examining the occurrence, mineral chemistry, and $^{208}Pb/^{232}Th$ ages of monazite and related minerals in pelitic schists from three well-characterized metamorphic terrains with relatively simple geologic histories. These include a Buchan (andalusite–sillimanite-type) terrain in south-central Maine, a Barrovian (kyanite–sillimanite-type) terrain in east-central Vermont, and a contact aureole in central Maine. Samples were collected from all metamorphic zones which range from the chlorite zone (all areas) to the kyanite zone (Barrovian terrain), sillimanite zone (Buchan terrain), or conditions of anatexis (contact aureole).

Geologic settings

All samples from the Buchan terrain are from the Waterville Formation (Fig. 1) that mostly consists of pelitic schist, micaceous quartzite, and minor marl interbedded on a scale of 2–10 cm. Occurrences of graptolites in the Waterville Formation and adjacent stratigraphic units define a Silurian (Llandovery) age of sedimentation (Tucker et al. 2001). The sediments were folded into isoclinally refolded recumbent folds and regionally metamorphosed during the Devonian Acadian orogeny (Osberg 1968, 1979, 1988). Regional metamorphism in the area has been reviewed by Osberg (1968, 1979, 1988) and Ferry (1994). Isograds were mapped in pelitic schists based on the appearance of biotite (Bt), garnet (Grt), andalusite (And), and sillimanite (Sil). (These and all other abbreviations for minerals follow Kretz 1983.) Staurolite (St) and cordierite (Crd) first appear in the And zone at or close to the And isograd. The P–T conditions at the peak of metamorphism were estimated from mineral equilibria in both pelitic schists and interbedded carbonate rocks. Pressure was 3.5 ± 0.5 kbar and T ranged from 400 ± 25 °C at the Bt isograd to 550 ± 25 °C in the Sil zone. Because porphyroblasts of Grt, And, St, and Crd have overgrown the axial plane foliation associated with the isoclinal folds, the peak of metamorphism postdated the peak of deformation. Novak and Holdaway (1981) suggested that two episodes of Acadian metamorphism occurred south and west of the area as shown in Fig. 1. If there were two Devonian metamorphic episodes in the area of Fig. 1, however, they were probably closely spaced in time and in P–T conditions (Holdaway et al. 1982). The metasediments are intruded by granite plutons that have Rb–Sr whole-rock ages of 385–395 Ma (Dallmeyer and van Breeman 1981). Zircon (Zrn) and sphene (Spn) from the plutons have U–Pb ages of 378–381 Ma (Tucker et al. 2001). Monazite (Mnz) and Zrn from a pegmatite immediately south of

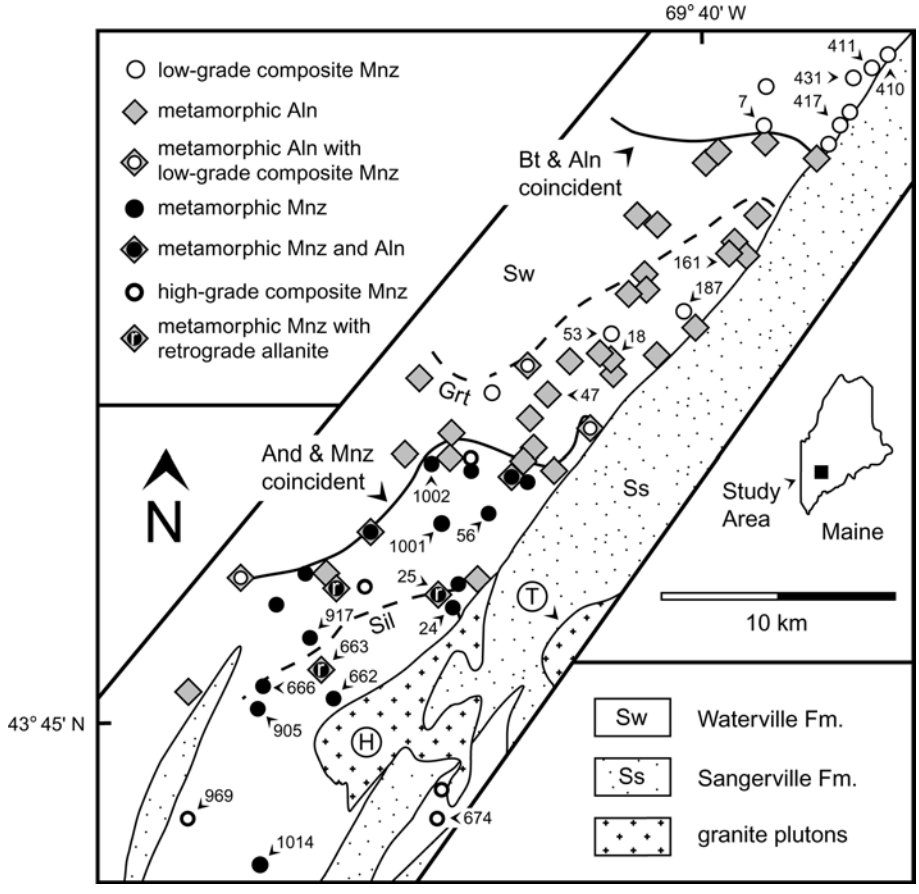

Fig. 1 Geologic sketch map of the Buchan regional metamorphic terrain in south-central Maine drawn from information in Osberg (1968, 1979, 1988) and Ferry (1976, 1981, 1984, 1987, 1994). *Data points* illustrate the distribution of allanite and monazite in pelitic schists from the Waterville Formation. A single sample was examined from each locality. *Numbers* refer to sample locations in text, tables, and other figures. *H* and *T* designate the Hallowell and Togus plutons, respectively

the area in shown in Fig. 1 at Gardiner, Maine, have a slightly younger U–Pb age, 367 Ma (Tucker et al. 2001). The close spatial association between the occurrence of clinozoisite and diopside in metacarbonate rocks and exposures of the granites suggests that plutonism and metamorphism were synchronous, or nearly so (Ferry 1976, 1983, 1994). Osberg (1988), however, argued on structural and other petrologic grounds that the peak of regional metamorphism post-dated emplacement of the granites.

Samples from the Barrovian terrain are from the Gile Mountain Formation (Fig. 2) that consists of pelitic schist, micaceous quartzite, and minor micaceous carbonate rock. Individual layers of sandstone and pelite range in thickness from ≈0.1 to 2 m; carbonate layers are thinner, ≈2–50 cm. The sedimentation age of the Gile Mountain Formation is Siluro-Devonian based on a 425 ± 5 Ma $^{40}Ar/^{39}Ar$ age for hornblende (Hbl) in a single sample from the formation (Spear and Harrison 1989) and the occurrence of Devonian plant fossils (Hueber et al. 1990). The Gile Mountain and underlying Waits River Formations were folded into recumbent folds and structural domes and regionally metamorphosed during the Devonian Acadian orogeny (Thompson et al. 1968; Thompson and Norton 1968; Osberg et al. 1989). Isograds were mapped in pelitic schists based on the appearance of Bt, Grt, and kyanite (Ky) (Lyons 1955). Staurolite first appears in the Grt zone close to the Ky isograd (Fig. 2; Ferry 1994). The P–T conditions at the peak of metamorphism were estimated from mineral equilibria in pelitic schists from both the Gile Mountain and Waits River Formations (Ferry 1994). Pressure was 8 ± 1 kbar and T ranged from 475 ± 25 °C in the Bt zone to 550 ± 25 °C in the Ky zone. Similar P–T estimates for the area were obtained by Menard and Spear (1993, 1994). Because porphyroblasts of St and Ky have overgrown the axial plane foliation associated with the recumbent folds, the peak of metamorphism post-dated recumbent folding and was contemporaneous with or slightly pre-dated development of the domes (Barnett and Chamberlain 1991; Menard and Spear 1994). There are no dated plutonic rocks in the area of Fig. 2. The Standing Pond volcanics member of the Waits River Formation is a thin, discontinuous stratigraphic unit at the boundary between the Waits River and Gile Mountain Formations (not shown on Fig. 2 for clarity). Hornblendes from the Standing Pond volcanics near the area of Fig. 2 have Acadian $^{40}Ar/^{39}Ar$ ages in the range 350–397 Ma (Spear and Harrison 1989).

Samples from the contact aureole are from the Devonian Carrabassett Formation (Fig. 3) that consists of metamorphosed pelites and graywackes interbedded on a scale of 1–100 cm (Osberg et al. 1985; Hanson and Bradley 1989). The Carrabasset Formation experienced isoclinal folding and chlorite-zone regional metamorphism followed by intrusion of the Onawa pluton during the Devonian Acadian orogeny. The Onawa pluton is a 2 by 5 km composite intrusion composed of quartz diorite and granodiorite. Concordant U–Pb ages of Zrn from the intrusion are 405 Ma (Bradley et al. 2000). Contact metamorphism of the Carrabassett Formation by the Onawa pluton has been described by Philbrick (1936), Moore (1960), and Symmes and Ferry (1995). Isograds in the pelitic rocks correspond to the appearance of And, And + K-feldspar (Kfs), and Sil. Biotite

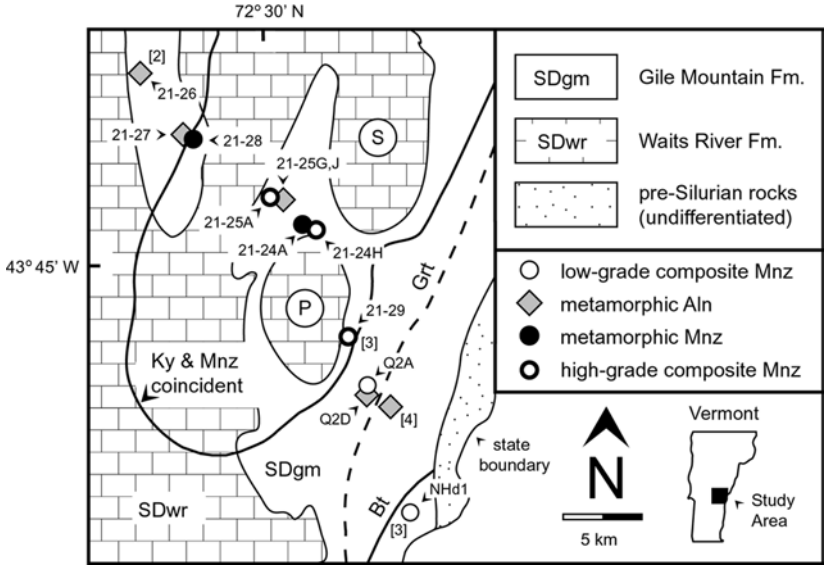

Fig. 2 Geologic sketch map of the Barrovian regional metamorphic terrain in east-central Vermont drawn from information in Lyons (1955), Doll et al. (1961), and Ferry (1994). *Data points* illustrate the distribution of allanite and monazite in pelitic schists from the Gile Mountain Formation. *Numbers in square brackets* indicate the number of samples examined from a locality, if more than one. *Other numbers* refer to sample locations in text, tables, and other figures. *Pairs of symbols* at locations 21–24, 21-25, and Q2 indicate that different samples from the same location contain different trace minerals; letters identify the specific samples that contain a particular trace mineral. *P* and *S* designate the Pomfret and Strafford structural domes, respectively

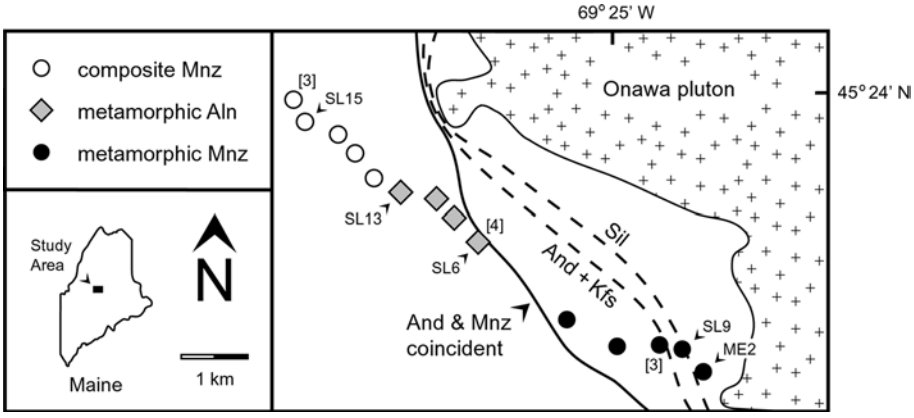

Fig. 3 Geologic sketch map of a portion of the Onawa contact aureole in central Maine (from Symmes and Ferry 1995). Data points illustrate the distribution of allanite and monazite in pelitic schists from the Carrabassett Formation. *Numbers in square brackets* indicate the number of samples examined from a locality, if more than one. *Other numbers* refer to sample locations in text and tables

and Crd first developed at the And isograd. Philbrick (1936) and Symmes and Ferry (1995) mapped an additional metamorphic zone at grades higher than the Sil isograd based on the appearance of leucocratic veins that contain crystallized partial melts (not represented on Fig. 3 for clarity). The P–T conditions at the peak of metamorphism were estimated from mineral equilibria in the pelitic rocks. Pressure was 3.0 ± 0.8 kbar and T ranged from 480–540 °C in the And zone to 640–650 °C in the zone of leucocratic veins with uncertainties of $\pm$10–20 °C. The absence of tectonic foliation in the pluton and the occurrence of And and Crd porphyroblasts that have overgrown foliation associated with the isoclinal folds indicate that emplacement of the pluton and contact metamorphism followed all or almost all deformation.

Methods of investigation

Eighty-two samples of pelitic rock from the Buchan terrain in Maine and 22 samples of pelite from the Barrovian terrain in Vermont were from earlier investigations (Ferry 1980, 1981, 1982, 1984, 1988, 1994). Twenty-one samples from the contact aureole in Maine were either from the study of Symmes and Ferry (1995) or from a new collection obtained along two traverses through the contact aureole. The sample set included specimens from each of the different metamorphic zones exposed in all three of the study areas. Multiple samples were examined from most locations in the Barrovian terrain and from three locations in the contact aureole.

Minerals were identified in polished thin sections of all samples with both optical petrography and backscattered electron (BSE) imaging supplemented by qualitative energy dispersive analysis using the JEOL JXA-8600 electron microprobe at Johns Hopkins University. Quantitative chemical analyses of Mnz and allanite (Aln) were measured with the electron microprobe using synthetic and natural mineral standards and a ZAF data correction scheme (Armstrong 1988). Accelerating voltage was 25 kV, beam current was 20 nA, and count times were $\approx$45 s. X-ray intensities for La, Ce, Gd, Ho, Er, Yb, Y, and Pb were measured at the Lα1 X-ray lines; intensities for Pr, Sm, Nd, and Dy were measured at the Lβ1 lines; and intensities for Th and U were measured at the Mα1 lines. An empirical correction scheme applied to raw intensities accounted for peak overlaps among the elements of concern.

Modal amounts of Mnz, Aln, and xenotime (Xen) in selected samples were measured with ultra-high precision using digital BSE images and a commercial image analysis package. The area of every Mnz, Aln, and Xen grain (typically 100–500 grains) was measured in a 1.5×1.5-mm region in thin section. Mode was computed as the total area of each mineral type divided by the area of the thin section surveyed.

Some major-element whole-rock chemical analyses were from earlier studies (Ferry 1981, 1982, 1984, 1988, 1994). These were supplemented by new whole-rock major- and trace-element analyses obtained commercially by X-ray fluorescence spectrometry and inductively coupled plasma mass spectrometry, respectively, at XRAL Laboratories, Toronto, Ontario.

$^{208}Pb/^{232}Th$ ages were measured for Mnz in situ in thin section for 19 samples using a CAMECA ims 1270 ion microprobe at UCLA, following procedures described by Harrison et al. (1995, 1999) and Hacker et al. (2000). Monazite grains, typically 20–30 μm in diameter, were located for analysis using BSE imaging of polished thin sections. Chips $\approx$5–20 mm^2, containing suitable grains, were sawed from thin sections and mounted in epoxy with pre-polished grains of Mnz age standard 554 (45 ± 1 Ma; Harrison et al. 1995, 1999). The mount was cleaned in successive baths of soap solution and distilled water, blown dry, and coated with $\approx$50 Å of Au. Unknown and standard Mnz grains were bombarded with a primary O_2^- beam, typically 5–15 μm in diameter with a current of 2–20 nA. A mass resolving power $\approx$4,500 separated all molecular interferences in the 204–208 mass range. An aperture was placed in the beam path to restrict secondary ions emitted from close to the edge of the sputtered crater to reduce common Pb contamination. Values of $^{232}ThO_2/^{232}Th$ and $^{208}Pb^*/^{232}Th$, determined with the ion microprobe for Mnz age standard 554, plot as a linear calibration curve. The calibration curve and the known $^{208}Pb^*/^{232}Th$ of the standard define

a relative sensitivity factor that was then used to determine the age of unknown Mnz grains analyzed under identical conditions. The reproducibility of the calibration curve typically was ±2% (cf. Harrison et al. 1995, 1999; Grove and Harrison 1999). Measured values of $^{232}ThO_2/^{232}Th$ and $^{208}Pb^*/^{232}Th$ for almost all Mnz dated in this study were in the range of values for Mnz standard 554 that defined the calibration curve. Age calculations assumed a common $^{208}Pb/^{204}Pb$ of 36.7, although the correction was typically small.

The uncertainty in individual measured Th–Pb ages was estimated from 215 measurements of the age of Mnz standard 554, obtained over two 1-week analytical sessions separated by 6 months. (Ages of no other Mnz standards were measured.) The 215 measurements varied about the mean age of Mnz standard 554, 45 Ma, with a pooled standard deviation of 0.77 Ma or 1.7% of the mean (pooled standard deviation of all measurements calculated following Jasper 2001). The calculated pooled standard deviation should be the best estimate of the standard deviation of a single Th–Pb age measurement of standard 554 (Jasper 2001). The reported value for each Th–Pb age of the unknowns is typically the mean of 15 measurements of $^{232}ThO_2/^{232}Th$ and $^{208}Pb^*/^{232}Th$ at one spot. In order to compare the age measurements in different analytical sessions, we considered the relative standard deviation of each Th–Pb measurement of an unknown to be the same as the relative standard deviation determined for the measured mean age of Mnz standard 554. The standard deviation of measured ages of individual spots, therefore, is reported as ±1.7% of the mean.

Whole-rock chemistry

Representative whole-rock compositions of samples considered in this investigation from the two regional terrains are listed in Table 1; analyses for rocks examined from the contact aureole have been published elsewhere (Table 3 of Symmes and Ferry 1995). The range in composition of all analyzed samples used in the study is summarized in Table 2. The composition of samples from the regional terrains cluster on a Thompson AFM diagram around several reference shale compositions (Fig. 4). The range in composition of rocks from the contact aureole lies within the range of whole-rock compositions from the regional terrains (Table 2). In terms of the AFM diagram, all samples investigated therefore have the chemistry of normal pelitic schists. The oxide component not considered by the AFM diagram that displays the widest variation is CaO. As discussed below, differences in CaO-content exert a significant control on the stability of Mnz and related minerals in pelitic schists from the regional terrains.

Table 1 Representative whole-rock compositions[a]

	Buchan terrain, south-central Maine							Barrovian terrain, east-central Vermont			
Sample	7	53	47	666	969	674	663	Q2A	21-27	21-25A	21-28
Zone	Chl	Grt	Grt	Sil	Sil	Sil	Sil	Grt	Grt	Ky	Ky
Tr Min[b]	Mnz	Mnz	Aln	Mnz	Mnz	Mnz	Aln/Mnz[c]	Mnz	Aln	Mnz	Mnz
SiO_2	52.30	54.20	53.90	50.85	75.05	57.38	42.22	72.00	54.70	69.70	60.20
Al_2O_3	18.90	21.80	19.20	22.10	11.60	18.76	26.46	11.80	23.70	13.40	16.50
CaO	2.51	0.30	2.45	2.20	0.51	1.27	3.47	0.69	0.98	1.60	1.98
MgO	4.24	2.33	4.79	5.02	1.59	4.78	4.92	3.17	2.37	2.28	3.07
Na_2O	2.01	0.68	3.03	2.18	1.35	1.33	2.02	1.38	1.36	2.60	1.99
K_2O	3.21	5.61	3.69	4.39	2.44	4.28	4.88	2.83	4.71	2.39	2.71
Fe_2O_3	8.59	9.52	9.23	9.88	5.98	8.20	12.35	5.80	7.87	5.43	10.20
MnO	0.53	0.34	0.13	0.20	0.06	0.17	0.34	0.08	0.11	0.16	0.29
TiO_2	0.82	1.01	0.84	1.00	0.69	0.84	1.21	0.64	1.14	0.99	0.98
P_2O_5	0.08	0.11	0.09	0.11	0.11	0.14	0.22	0.14	0.13	0.14	0.17
Cr_2O_3	0.03	0.04	0.04	0.04	0.06	0.00	0.00	0.02	0.07	0.04	0.03
LOI	6.70	2.85	1.30	1.55	0.80	1.83	1.32	1.39	2.95	1.08	1.93
Total	99.92	98.79	98.69	99.52	100.24	98.98	99.41	99.94	100.09	99.81	100.05
Ca/Ca_{Shaw}	1.15	0.14	1.12	1.01	0.23	0.58	1.59	0.32	0.45	0.73	0.91
Al/Al_{Shaw}	1.14	1.31	1.16	1.33	0.70	1.13	1.59	0.71	1.43	0.81	0.99
La	38.2	65.3	34.2	28.1	29.6	n.d.[d]	n.d.[d]	n.d.[d]	71.7	26.8	28.1
Ce	80.5	137.0	68.3	58.2	62.6	n.d.[d]	n.d.[d]	n.d.[d]	137.0	57.9	61.3
Pr	8.7	14.8	8.0	7.0	7.2	n.d.[d]	n.d.[d]	n.d.[d]	16.2	6.7	7.1
Nd	31.9	54.7	27.5	27.7	28.0	n.d.[d]	n.d.[d]	n.d.[d]	63.1	27.0	29.0
Sm	5.7	9.3	4.3	5.7	5.7	n.d.[d]	n.d.[d]	n.d.[d]	11.2	5.4	5.8
Gd	4.9	8.4	3.6	5.3	5.6	n.d.[d]	n.d.[d]	n.d.[d]	10.1	5.4	6.4
Dy	4.5	8.6	3.9	5.1	5.3	n.d.[d]	n.d.[d]	n.d.[d]	8.3	5.2	5.8
Y	21.0	44.0	19.0	20.0	25.0	n.d.[d]	n.d.[d]	n.d.[d]	38.0	26.0	28.1
Er	2.4	4.9	2.5	2.8	2.9	n.d.[d]	n.d.[d]	n.d.[d]	4.3	3.1	3.3
Yb	2.3	4.9	2.1	2.7	3.0	n.d.[d]	n.d.[d]	n.d.[d]	3.8	3.0	3.3
Th	13.4	26.7	14.8	11.4	10.2	n.d.[d]	n.d.[d]	n.d.[d]	20.4	9.5	9.6
U	2.4	4.6	2.1	2.4	2.9	n.d.[d]	n.d.[d]	n.d.[d]	4.6	2.7	2.8

[a]Major elements reported in oxide wt% with all Fe as Fe_2O_3. Trace elements reported in ppm.(Ca/Ca_{Shaw}) and (Al/Al_{Shaw}) are with respect to Shaw's (1956) average low-grade pelite (CaO = 2.18% and Al_2O_3 = 16.62%)

[b]*Tr Min* Diagnostic trace mineral

[c]Sample contains Mnz–Aln intergrowths with Aln considered retrograde after metamorphic Mnz

[d]*n.d.* Not determined

Table 2 Range in whole-rock compositions of all analyzed samples[a]

	Buchan terrain, south-central Maine			Barrovian terrain, east-central Vermont			Contact aureole, central Maine		
	Max.	Min.	Avg.	Max.	Min.	Avg.	Max.	Min.	Avg.
SiO_2	73.80	32.40	54.14	72.00	41.90	60.04	69.60	58.60	63.67
Al_2O_3	26.46	11.60	19.31	27.00	10.60	16.68	19.50	14.80	17.70
CaO	10.40	0.28	2.56	11.60	0.69	2.31	0.86	0.27	0.46
MgO	6.42	1.59	4.20	5.79	2.28	3.59	2.32	1.51	1.87
Na_2O	3.36	0.42	1.82	2.82	0.62	1.82	2.06	1.05	1.36
K_2O	5.64	2.32	3.98	6.69	2.39	3.71	3.72	2.76	3.32
Fe_2O_3	15.90	5.98	9.57	11.80	5.24	7.55	8.00	6.16	7.15
MnO	5.08	0.06	0.48	0.44	0.07	0.17	0.10	0.06	0.08
TiO_2	1.23	0.69	0.92	1.38	0.48	0.91	1.04	0.88	0.99
P_2O_5	1.20	0.07	0.16	0.17	0.02	0.13	0.17	0.12	0.15
Cr_2O_3	0.06	0.00	0.02	0.07	0.01	0.03	0.05	0.03	0.04
LOI	7.57	0.34	2.00	9.31	0.85	2.68	3.60	0.85	2.48
Total			99.15			99.83			99.25

[a]Values in oxide wt% with all Fe as Fe_2O_3 and include analyzed samples from all grades in each terrain

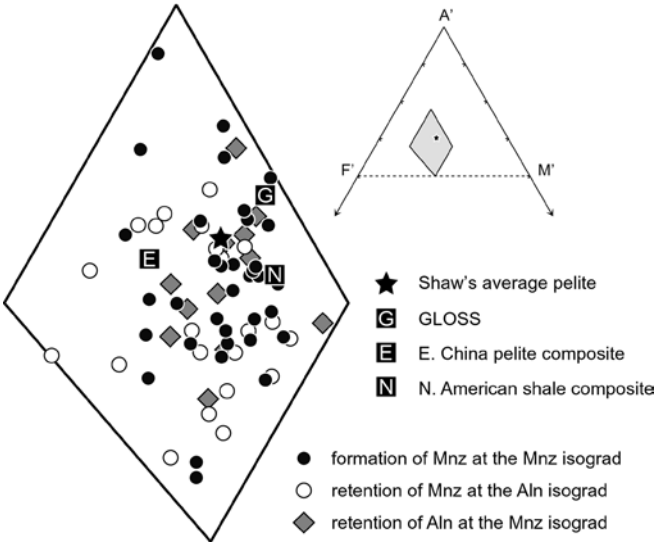

Fig. 4 Thompson (1957) AFM diagram illustrating the whole-rock composition of all analyzed samples considered in this study from the Buchan and Barrovian regional metamorphic terrains. *Inset* shows the range of composition space represented by the main portion of the diagram. *Symbols* refer to the plotting position of the samples on Figs. 7 and 8. Reference shale and pelite compositions shown for comparison are Shaw's (1956) average low-grade pelite, the global subducting sediment (GLOSS) of Plank and Langmuir (1998), the post-Archean east China pelite composite of Gao et al. (1998), and the North American shale composite of Gromet et al. (1984). Samples used in the study are normal pelitic rocks in terms of chemical variables considered by the AFM diagram. In terms of the AFM diagram there is no significant difference in composition among pelites that contain insufficient Ca and/or Al to stabilize allanite in the biotite and garnet zones, pelites that develop monazite from allanite at the andalusite or kyanite isograd, and pelites that contain sufficient Ca and/or Al to stabilize allanite in the andalusite or kyanite zone

Mineralogy, mineral distributions, and mineral chemistry

Buchan terrain, south-central Maine

Reactions in which Mnz participated during prograde metamorphism of pelitic schists likely involved other minerals rich in P and/or REE. In pelites from the Waterville Formation, these include Aln, Xen, and apatite (Ap). Apatite occurs in every sample examined. Although Xen was observed in every metamorphic zone except the Grt zone, it occurs in only 17% of the samples and in concentrations one to two orders of magnitude less than that of Mnz. Xenotime, therefore, probably was an unimportant participant in reactions involving Mnz. Figure 1 illustrates the distribution of Mnz and the remaining mineral of interest, Aln, in pelitic schists from the Waterville Formation. At grades lower than the Bt isograd, all samples in the chlorite (Chl) zone contain Mnz (Fig. 5A) and are devoid of Aln. With increasing grade, Mnz disappears precisely at the Bt isograd and is replaced by euhedral porphyroblasts of metamorphic Aln (Fig. 5B). Minute grains of a $ThSiO_4$ mineral, probably thorite, are commonly closely associated spatially with the Aln. With the exception of six samples, pelites from the Bt and Grt zones contain Aln, but no Mnz. With further increase in grade, Aln disappears from most samples precisely at the And isograd and is replaced by Mnz. Monazite in the And zone close to the And isograd occurs as fine-grained clusters about the same size as Aln porphyroblasts in the Bt and Grt zones (Fig. 5C). At higher grades, Mnz forms isolated grains (Fig. 5D). With the exception of three samples, pelites from the Sil zone contain Mnz but no Aln. In the exceptions (Fig. 1), Aln occurs as a reaction rim on Mnz and appears to be retrograde rather than prograde.

Monazite in the Chl and Grt zones differs in both texture and chemical composition from Mnz in the And and Sil zones. Monazite from the Chl and Grt zones is composed of an irregular, inclusion-choked rim surrounding an inclusion-free core that has a regular outline (Fig. 5A). Core and rim differ slightly in BSE brightness that primarily results from differences in Th contents. As is typical for Mnz from metamorphic rocks, Mnz from the Chl and Grt zones is enriched in LREE relative to Y, Ca, Th, U, Pb, and the HREE (Tables 3, 4, Fig. 6). In contrast, most Mnz grains in pelitic schists from the And and Sil zones have subhedral idioblastic forms, contain few or

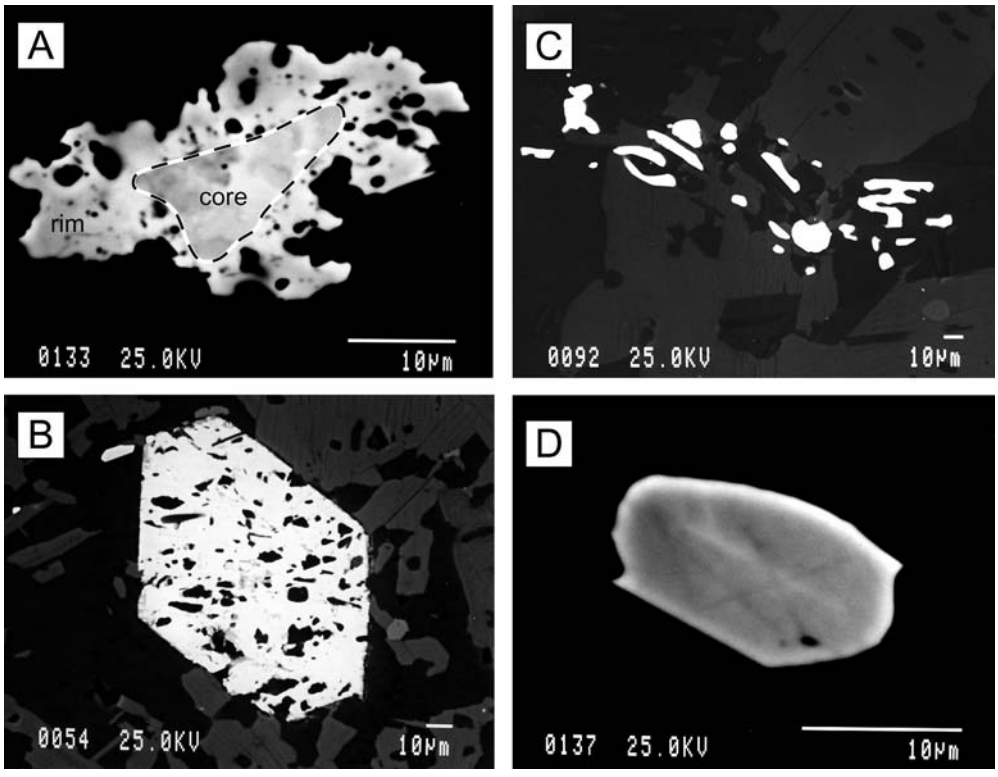

Fig. 5A–D Back-scatted electron (BSE) photomicrographs of monazite and allanite in pelitic schists from the Waterville Formation in the Buchan terrain, south-central Maine. Matrix silicates appear dark in all photos. **A** Representative composite monazite (bright mineral) in sample 410 from the chlorite zone with inclusion-free core surrounded by highly irregular inclusion-choked rim. Inclusions in monazite are primarily quartz. **B** Representative metamorphic allanite porphyroblast (large bright mineral) in sample 18 from the garnet zone. Inclusions in allanite are primarily quartz. **C** Cluster of metamorphic monazite grains (bright minerals) in sample 917 from the andalusite zone. The size of the cluster is similar to that of porphyroblasts of metamorphic allanite observed at lower grades. **D** Representative isolated metamorphic monazite (bright mineral) in sample 24 from the sillimanite zone with idioblastic form and almost no chemical zonation (the bright rim is an artifact of BSE imaging rather than compositional zoning)

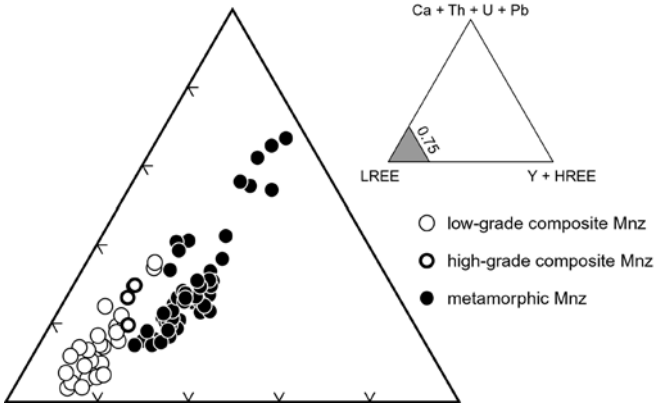

Fig. 6 Chemical composition of monazite from pelitic schists from the Waterville Formation in the Buchan terrain, south-central Maine. High-grade composite monazite distinguished from metamorphic monazite by whole-rock chemistry (Fig. 7). Compositions of composite and metamorphic monazites define non-overlapping fields. The difference in composition may be used to discriminate between composite and metamorphic monazite in samples at grades above the monazite isograd

no inclusions, and, almost without exception, display little or no chemical zoning in BSE imaging (Fig. 5D). Most Mnz from the And and Sil zones contains higher concentrations of Y, Ca, Th, Pb, and HREE and lower concentrations of LREE compared with Mnz from the Chl and Grt zones (Tables 3, 4, Fig. 6). On the basis of texture, mineral chemistry, and distribution in the field, Mnz in pelites from the Waterville Formation, therefore, can be divided into two populations. Monazites from the Chl and Grt zones will be referred to as "composite" because they have inclusion-free cores and inclusion-rich rims with contrasting BSE brightness. The subhedral, unzoned, inclusion-free Mnz grains in the And and Sil zones will be referred to as "metamorphic" Mnz because they appear to have replaced metamorphic Aln by a prograde mineral reaction. As will be documented below, however, some Mnz in the And and Sil zones is composite Mnz that persisted from conditions of the Chl, Bt, and Grt zones into conditions at higher grade (and recrystallized to varying degrees).

The occasional survival of composite Mnz in the Grt zone and of Aln in the And zone can be explained by differences in whole-rock Ca and Al contents. The Ca and Al contents of all analyzed samples from the Bt and Grt zones of the Buchan and Barrovian terrains are plotted in Fig. 7 relative to the composition of Shaw's (1956) average pelite. Samples with Aln, but not composite Mnz, lie in a field of the diagram distinct from the field for samples

Table 3 Composition of composite monazite[a] in selected samples[b]

Terrain	Buchan	Buchan	Buchan	Buchan	Barrovian	Aureole	Aureole
Sample	411	431	53[c]	969[c]	NHd1O	SL15	SL19[d]
Zone	Chl	Chl	Grt	Sil	Chl	Chl	Chl
Type[e]	C	C	C	C	C	C	C
Si	0.026	0.027	0.042	0.006	0.023	0.008	0.019
P	1.005	1.007	0.998	0.992	0.984	1.008	0.999
Ca	0.014	0.009	0.016	0.033	0.012	0.010	0.005
La	0.151	0.186	0.223	0.205	0.215	0.155	0.209
Ce	0.478	0.451	0.438	0.451	0.428	0.452	0.438
Pr	0.050	0.049	0.044	0.046	0.048	0.055	0.048
Nd	0.191	0.175	0.153	0.167	0.174	0.222	0.183
Sm	0.031	0.023	0.021	0.035	0.028	0.037	0.034
Gd	0.023	0.018	0.016	0.013	0.045	0.026	0.032
Dy	0.002	0.002	0.002	0.005	0.004	0.004	0.005
Er	0.000	0.000	0.000	0.001	0.000	0.000	0.000
Y	0.011	0.007	0.010	0.016	0.013	0.015	0.014
Pb	0.000	0.001	0.001	0.001	0.000	0.000	0.000
Th	0.007	0.025	0.021	0.028	0.023	0.002	0.003
U	0.000	0.000	0.000	0.004	0.000	0.000	0.000
Oxide sum	100.09	99.92	100.09	100.10	99.94	99.54	99.82

[a]Monazite: cationsper four oxygen atoms
[b]Reported values are typically the average of two to three spot analyses of three to four grains in thin section. Oxide sum is the sum of the wt% of metal oxides with all Fe asFeO
[c]Monazite in samples53 and 969 is considered composite based on mineral composition and whole-rock chemistry
[d]Sample SL19 was collected from the lowest grade portion of the contact aureole south of the pluton outside Fig. 3
[e]*C* Composite; *M* metamorphic

Table 4 Composition of metamorphic monazite[a] in selected samples[b]

Terrain	Buchan	Buchan	Buchan	Buchan	Barrovian	Aureole	Aureole
Sample	56	1001	905	662	21-28	SL9	ME2
Zone	And	And	Sil	Sil	Ky	And + Kfs	And + Kfs
Type[c]	M	M	M	M	M	M	M
Si	0.015	0.010	0.009	0.011	0.005	0.019	0.030
P	1.000	1.003	1.006	1.006	0.998	0.999	0.992
Ca	0.053	0.030	0.029	0.034	0.030	0.033	0.042
La	0.197	0.166	0.216	0.206	0.190	0.196	0.195
Ce	0.403	0.403	0.420	0.417	0.395	0.400	0.393
Pr	0.046	0.046	0.044	0.044	0.048	0.043	0.041
Nd	0.152	0.198	0.157	0.152	0.171	0.159	0.151
Sm	0.025	0.043	0.024	0.023	0.031	0.028	0.025
Gd	0.027	0.034	0.023	0.024	0.049	0.026	0.024
Dy	0.004	0.007	0.007	0.007	0.010	0.009	0.008
Er	0.000	0.000	0.001	0.001	0.001	0.002	0.002
Y	0.021	0.031	0.028	0.034	0.039	0.055	0.057
Pb	0.001	0.001	0.001	0.001	0.001	0.001	0.001
Th	0.052	0.023	0.025	0.031	0.028	0.022	0.032
U	0.002	0.002	0.002	0.002	0.005	0.004	0.003
Oxide sum	99.95	100.08	99.68	100.15	99.84	100.13	100.19

[a]Monazite: cationsper four oxygen atoms
[b]Reported values are typically the average of two to three spot analyses of three to four grains in thin section. Oxide sum is the sum of the wt% of metal oxides with all Fe asFeO
[c]*C* Composite; *M* metamorphic

that contain composite Mnz without Aln. A line separating the two fields was drawn by inspection on Fig. 7 whose position and slope are primarily constrained by data for two of the samples with both Aln and Mnz and by the datum for sample 53. A third sample with Aln and Mnz for unknown reasons is the single exception to stability fields for Aln and Mnz defined by the line in Fig. 7. Allanite evidently developed from composite Mnz at the Bt isograd only in pelites that contain average or above-average Ca and/or Al contents. There was insufficient Ca and/or Al to produce Aln in the few pelites with below-average Ca and/or Al contents. Composite Mnz then was able to persist in these samples at grades higher than the Bt isograd. The Ca and Al contents of analyzed samples from the And, Ky, and Sil zones of the Buchan and Barrovian terrains are plotted in Fig. 8 relative to the composition of Shaw's (1956) average pelite as well. Samples with Aln, but not Mnz, lie in a field of the diagram distinct from samples that contain Mnz with and without Aln. A line separating the two fields was drawn by inspection on Fig. 8 whose position and slope are primarily constrained by the two data points that lie on the line and by the datum for sample 21-25J. Allanite evidently was stabilized during metamorphism by elevated whole-rock Ca and/or Al contents and persisted in these samples into the And zone (and Ky zone of the Barrovian terrain).

Figure 7 provides a simple way to discriminate between composite and metamorphic Mnz in the And and Sil zones (and in the Ky zone of the Barrovian terrain). Samples whose whole-rock composition lies below the discrimination line in Fig. 7 contain composite rather than metamorphic Mnz. On this basis, occurrences of composite Mnz in the And and Sil zones were distinguished in Figs. 1 and 8 from occurrences of metamorphic Mnz (the specific case of sample 674 is discussed further below). Monazite from the And and Sil zones (and from the Ky zone of the Barrovian terrain) that was identified as composite on the basis of Fig. 7 is re-

Table 5 Composition of allanite[a] in selected samples[b]

Terrain	Buchan	Buchan	Buchan	Barrovian	Aureole	Aureole
Sample	47	18	1001[c]	21-26	SL6C	SL13
Zone	Grt	Grt	And	Grt	Chl	Chl
Type[d]	M	M	M	M	M	M
Ca	1.339	1.262	1.395	1.206	1.079	1.083
Mn	0.040	0.062	0.058	0.019	0.030	0.017
La	0.129	0.142	0.079	0.154	0.194	0.194
Ce	0.263	0.316	0.191	0.334	0.388	0.413
Pr	0.031	0.035	0.024	0.036	0.045	0.032
Nd	0.103	0.123	0.099	0.127	0.164	0.157
Sm	0.018	0.019	0.023	0.023	0.029	0.028
Gd	0.017	0.015	0.020	0.036	0.020	0.025
Dy	0.006	0.004	0.007	0.005	0.005	0.006
Er	0.002	0.002	0.002	0.002	0.002	0.001
Y	0.026	0.018	0.040	0.015	0.026	0.026
Pb	0.001	0.000	0.001	0.003	0.001	0.000
Th	0.003	0.005	0.005	0.010	0.008	0.013
U	0.000	0.000	0.000	0.001	0.000	0.000
Al	2.143	2.165	2.307	2.141	2.085	2.012
Fe^{3+}	0.169	0.120	0.165	0.062	0.015	0.061
Fe^{2+}	0.632	0.654	0.507	0.765	0.885	0.905
Mg	0.036	0.040	0.062	0.041	0.020	0.019
Ti	0.045	0.022	0.004	0.036	0.009	0.006
Si	2.997	2.992	3.012	2.984	2.995	3.002
Oxide sum	98.03	98.51	97.46	99.44	99.38	97.87

[a]Illanite: cations per eight cations with Fe^{3+}/Fe^{2+} adjusted to balance 12.5 oxygen atoms
[b]Reported values are typically the average of two to three spot analyses of three to four grains in thin section. Oxide sum is the sum of the wt% of metal oxides with all Fe asFeO
[c]Allanite in sample 1001 occurs only as inclusions in garnet
[d]*C* Composite; *M* metamorphic

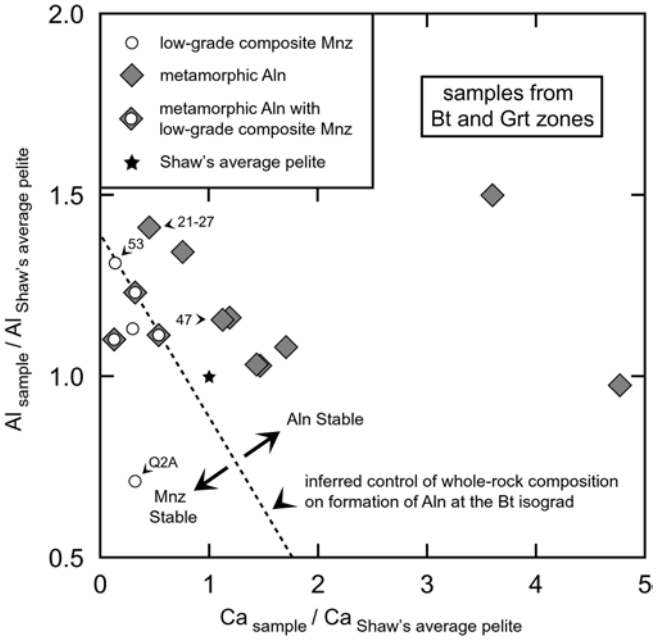

Fig. 7 Whole-rock Ca and Al contents of all analyzed pelitic schists from the biotite and garnet zones of the Buchan and Barrovian regional metamorphic terrains. Values are referenced to Shaw's (1956) average pelite. Data points for samples with allanite, but not monazite, lie in a region distinct from the area for samples with monazite, but not allanite. Composite monazite evidently was stabilized during regional metamorphism at conditions of the biotite and garnet zones in samples with below-normal Ca and/or Al contents, accounting for occurrences of monazite in the biotite and garnet zones of both regional terrains. The discrimination line illustrates the relationship between whole-rock composition and the stability of monazite and allanite only for metamorphic conditions of the biotite and garnet zones. *Numbers* refer to sample locations in text, tables, and other figures

ferred to in the text and figures as "high-grade" composite Mnz. Monazite from the Chl, Bt, and Grt zones is referred to as "low-grade" composite Mnz.

Lines in Figs. 7 and 8 that define the control of whole-rock composition on the development of Aln and Mnz in pelitic schists have positions that depend in detail both on the values of a variety of chemical variables attained during metamorphism such as P, T, and the activity of H_2O and on the mineral reactions that produce Aln and Mnz. Figures 7 and 8, therefore, may have limited predictive capability except for conditions and reactions like those at or near the Bt isograd (Fig. 7), or at the And or Ky isograds (Fig. 8) of the two regional terrains investigated in this study. A case in point is the contact aureole in central Maine where all analyzed Aln-bearing samples lie within the Mnz stability field on Fig. 7 because the Aln-forming reaction in the aureole differs from that in the regional terrains. Diagrams such as Figs. 7 and 8, however, show more promise in representing the control of bulk rock composition on the stability of Aln and Mnz than do conventional diagrams used for graphical analysis of phase equilibria in pelitic schists (Fig. 4).

Figure 9 illustrates the distribution of Mnz and Aln in pelitic schists with the following samples omitted: (1) those from the Grt zone that contain composite Mnz stabilized by relatively low whole-rock Ca and/or Al contents (i.e., those below the discrimination line in Fig. 7), (2) those from the And zone that contain Aln stabilized by relatively high whole-rock Ca and/or Al contents (i.e., those above the upper discrimination line in Fig. 8), and (3) those from the And and Sil zones that contain retrograde Aln after metamorphic Mnz. The "filtered" distribution map makes clear that, within the resolution of the sample set, (1) the Bt isograd coincides with an Aln isograd at which metamorphic Aln replaces composite Mnz in most rocks by one prograde mineral reaction, and (2) the And isograd coincides with a Mnz isograd at which metamorphic Mnz replaces metamorphic Aln in most rocks by a second prograde reaction.

Barrovian terrain, east-central Vermont

The distribution of Mnz and Aln in pelitic schists from the Barrovian terrain (Fig. 2) is the same as in the Buchan terrain. At grades lower than the Bt isograd pelites contain Mnz, but not Aln. Monazite in the Chl zone has the same texture as composite Mnz from the Waterville Formation and the same relatively low contents of Y, Ca, Th, U, Pb, and HREE compared with Mnz at higher grade (Tables 3, 4). All but one sample from the Bt and

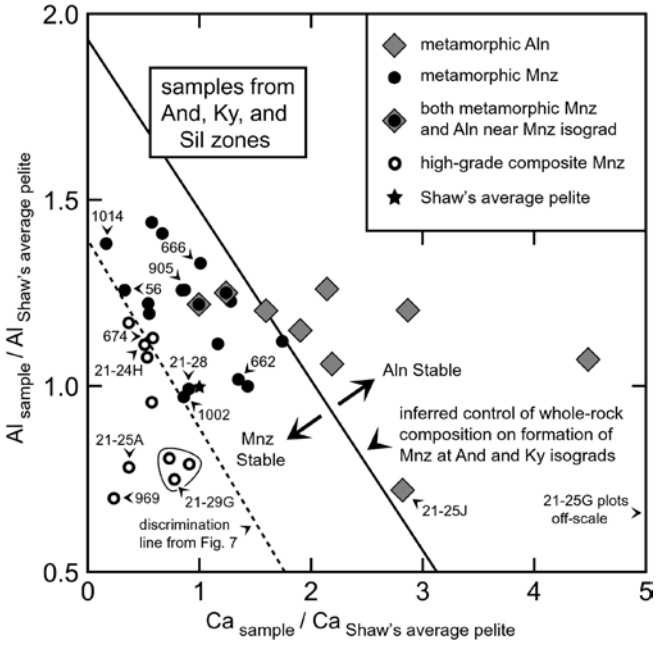

Fig. 8 Whole-rock Ca and Al contents of pelitic schists from the andalusite, kyanite, and sillimanite zones of the Buchan and Barrovian regional metamorphic terrains omitting the three samples from the Buchan terrain with metamorphic monazite partially replaced by retrograde allanite. Values are referenced to Shaw's (1956) average pelite. Data points for samples with allanite but not monazite lie in a region at elevated Ca and/or Al distinct from the region for samples with monazite (with and without allanite). Metamorphic allanite evidently was stabilized during regional metamorphism at conditions of the andalusite and kyanite zones in samples with above-normal Ca and/or Al contents, accounting for occurrences of allanite in the andalusite and kyanite zones of both regional terrains. The upper discrimination line illustrates the relationship between whole-rock composition and the stability of monazite and allanite only for metamorphic conditions at and near the andalusite and kyanite isograds. The lower discrimination line from Fig. 7 was used to distinguish between occurrences of composite and metamorphic monazite from the andalusite, kyanite, and sillimanite zones. The specific case of sample 674 is discussed in the text. *Numbers* refer to sample locations in text, tables, and other figures. The *thin line* around sample 21-29G and the two closest data points for composite monazite indicates that all three samples are from location 21-29 in the Barrovian terrain

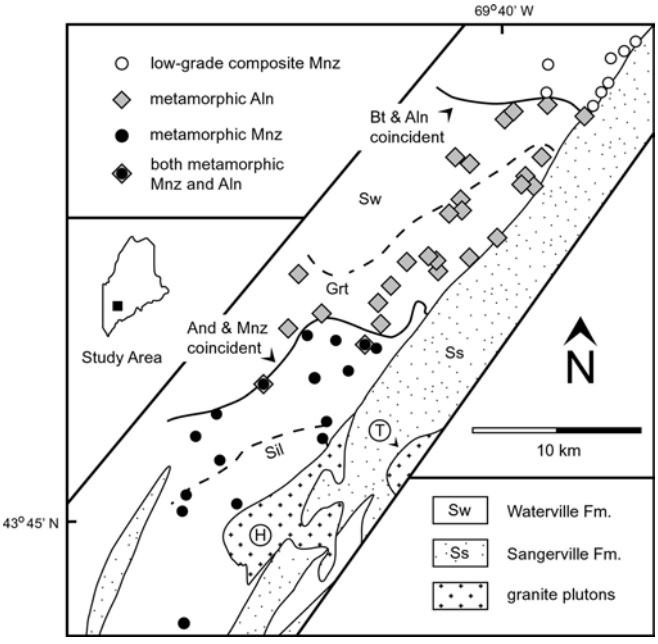

Fig. 9 Geologic sketch map of the Buchan terrain, south-central Maine, showing the distribution of composite and metamorphic monazite and metamorphic allanite in pelitic schists from the Waterville Formation omitting samples from the garnet, andalusite, and sillimanite zones in which composite monazite was stabilized by below-normal whole-rock Ca and/or Al contents; samples from the andalusite zone in which metamorphic allanite was stabilized by above-normal whole-rock Ca and/or Al contents; and samples from the sillimanite and andalusite zones with retrograde allanite after monazite. The "filtered" distribution of minerals makes clear that isograds for the prograde development of metamorphic allanite and monazite coincide with isograds for the prograde development of biotite and andalusite, respectively. Other features the same as in Fig. 1

Grt zones contain metamorphic Aln, but not Mnz. Monazite in the exception (sample Q2A) evidently was stabilized by relatively low whole-rock Ca and Al contents as was observed in the Buchan terrain (Table 1, Fig. 7). Most pelitic schists from the Ky zone contain Mnz, but not Aln. The exceptions are two samples (both at location 21-25) in which Aln was stabilized by elevated whole-rock Ca contents as was observed in the Buchan terrain (Fig. 8). Monazite in the Ky zone has subhedral idioblastic form and relatively high contents of Y, Ca, Th, U, Pb, and HREE compared with composite Mnz from the Chl zone (Tables 3, 4). The whole-rock Ca and Al contents of five samples, three from location 21-29 and one each from locations 21–24 and 21-25, however, indicate that they contain composite rather than metamorphic Mnz (Fig. 8). The remaining two samples from the Ky zone (21-24A, 21-28) contain metamorphic Mnz based on their whole-rock compositions. The Ky isograd coincides with a Mnz isograd at which prograde metamorphic Mnz replaces metamorphic Aln. Within the resolution of the sample set, the Bt isograd coincides with an Aln isograd at which prograde Aln replaces composite Mnz.

Contact aureole, central Maine

The distribution of Mnz and Aln in pelites from the contact aureole (Fig. 3) is almost identical to that in the Buchan and Barrovian terrains. Rocks contain Mnz, but not Aln, at the lowest grades exposed in the aureole. Monazite has the same textural and chemical characteristics as composite Mnz from the Buchan and Barrovian terrains (Tables 3, 4). With increasing grade of metamorphism, but at grades lower than the And isograd, composite Mnz disappears and is replaced by metamorphic Aln. All pelites from the And zone and at higher grades contain Mnz and are devoid of Aln. Monazite in the And, And + Kfs, and Sil zones has the same textural and chemical characteristics as

metamorphic Mnz from the Buchan and Barrovian terrains (Tables 3, 4). The And isograd coincides exactly with a Mnz isograd at which prograde Mnz replaces metamorphic Aln. Unlike in regional metamorphic terrains, there is no separate Bt isograd in pelitic rocks in contact aureoles (Pattison and Tracy 1991). Biotite typically first appears as a product of reactions that produce And and/or Crd. The Aln isograd in the contact aureole, therefore, cannot be correlated spatially with a separate Bt isograd as it can in the regional metamorphic terrains. Nevertheless, development of metamorphic Aln in the contact aureole is closely analogous to development of Aln in the regional terrains because it occurs at a grade of metamorphism lower than the And isograd.

Modes, whole-rock trace-element chemistry, and prograde mineral reactions

Monazite participated in two different prograde reactions during metamorphism of pelitic rocks in northern New England, one that produced Aln from Mnz and a second that produced Mnz at the expense of Aln. Prograde reactions at the Aln and Mnz isograds were inferred from a consideration of mass balance and petrologic relations. The mass balance constraints are presented in Tables 7, 8, 9 and Fig. 10. The fraction of selected REE, Y, Th, and U in whole-rock samples that is contained in Aln and Mnz was computed from measured whole-rock compositions (Table 1) and the compositions and modes of Aln and Mnz (Tables 3, 4, 5, 6). Results demonstrate that most of the LREE in individual samples of pelitic schist are contained in Aln or Mnz (Tables 7, 8, 9, Fig. 10). There is almost complete overlap in data for Y and all the analyzed REE (but not for Th and U) between Mnz and Aln as shown in Fig. 10. Other minerals in the rocks, therefore, were not significant sources or sinks for the LREE in the Aln- and Mnz-forming reactions, and all the REE were simply transferred locally from Mnz to Aln or vice versa during the reactions. The greater abundance of Th and U in Mnz than in Aln requires that Th and U were sited in a mineral other than Aln during the Aln-forming reaction and then were derived from that mineral during the Mnz-forming reaction.

The principal petrologic constraints on the nature of prograde reactions involving Mnz are (1) Ap is the only abundant phosphate other than Mnz (Xen is one to two orders of magnitude less abundant than Mnz, Table 6); (2) tiny $ThSiO_4$ grains are commonly closely associated spatially with Aln; and (3) the Aln- and Mnz-forming reactions coincide with the Bt and And or Ky isograds, respectively. $ThSiO_4$, Ap, and Bt, but not Xen, therefore, were significantly involved in the Aln-forming reaction. $ThSiO_4$, Ap, and And or Ky, but not Xen, were involved in the Mnz-forming reaction. Other major minerals in the pelites likely participated in the Aln- and Mnz-forming reactions as well.

In pelites with average or above-average Ca contents from the Buchan and Barrovian terrains, reactants of the Bt-forming reaction at the Bt isograd were muscovite (Ms), ankerite (Ank), siderite (Sd), and quartz (Qtz) (Ferry 1984, 1988). Using idealized mineral formulas, an Aln-forming reaction that conserves REE in Aln and Mnz and that is analogous to the Bt-forming reaction by producing Bt and a Ca–Al silicate (Aln) at the expense of Ms, Ank, Sd, and Qtz is:

$$\underset{\text{Mnz}}{3(\text{REE})\text{PO}_4} + \underset{\text{Ms}}{3\text{KAl}_3\text{Si}_3\text{O}_{10}(\text{OH})_2} + \underset{\text{Ank}}{8\text{Ca}(\text{Fe},\text{Mg})(\text{CO}_3)_2} + \underset{\text{Sd}}{4(\text{Fe},\text{Mg})\text{CO}_3} + \underset{\text{Qtz}}{9\text{SiO}_2} + 2\text{H}_2\text{O}$$
$$= \underset{\text{Aln}}{3(\text{CaREE})(\text{Al}_2\text{Fe})\text{Si}_3\text{O}_{12}(\text{OH})} + \underset{\text{Bt}}{3\text{K}(\text{Fe},\text{Mg})_3\text{AlSi}_3\text{O}_{10}(\text{OH})_2} + \underset{\text{Ap}}{\text{Ca}_5(\text{PO}_4)_3(\text{OH})} + 20\text{CO}_2.$$

Allanite formed in the contact aureole in rocks with Mu, Chl, Qtz, plagioclase (Pl), and calcite (Cal), but not Bt, Ank, or Sd. Using idealized mineral formulas, a possible Aln-forming reaction is:

Table 6 High-precision modes ofallanite, monazite, and xenotime in selected samples from the Buchan terrain, south-central Maine

Sample	161	47	56	917	24	666
Zone	Grt	Grt	And	And	Sil	Sil
Allanite mode[a]	0.04436(4)	0.05226(5)	n.p.[b]	n.p.[b]	n.p.[b]	n.p.[b]
Monazite mode[a]	n.p.[b]	n.p.[b]	0.01145(7)	0.01228(6)	0.01138(1)	0.01488(6)
Xenotime mode[a]	n.p.[b]	n.p.[b]	0.00027(1)	0.00069(2)	0.00040(2)	0.00107(2)
V_{Aln} (cm^3)[c]	143.22	143.22	–	–	–	–
V_{Mnz} (cm^3)[c]	–	–	45.13	45.07	45.02	45.06

[a]Values in volume %. See text for method of measurement; 1σ error in the last digit in parentheses
[b]n.p.Not present in sample
[c]Molar volumes calculated from unit cell parameters reported in Dollase (1971) for allanites and in Gratz and Heinrich (1997) for monazite

$$15(REE)PO_4 + 3Fe_5Al_2Si_3O_{10}(OH)_8 + 12CaAl_2Si_2O_8 + 28CaCO_3 + 12SiO_2$$
Mnz ChlPl Cal Qtz
$$= 15(CaREE)(Al_2Fe)Si_3O_{12}(OH) + 5Ca_5(PO_4)_3(OH) + 2H_2O + 28CO_2.$$
Aln Ap

Small amounts of $ThSiO_4$ must have been produced by both Aln-producing reactions to account for Th and U released from Mnz but not accommodated in Aln (Fig. 10). The two Aln-forming reactions involve decarbonation and were probably driven by infiltration of the pelitic rocks by a reactive aqueous fluid during metamorphism, as was the Bt-forming reaction at the Bt isograd in the regional terrains (Ferry 1984, 1988). The common driving mechanism then explains the coincidence between the Aln and Bt isograds.

The isograd at which Mnz developed from Aln coincides in each of the three areas with the first appearance of And or Ky. Monazite also developed in pelites at this grade of metamorphism in rocks that contain St (regional terrains) or Crd (Buchan terrain and contact aureole), but not And or Ky. The development of metamorphic Mnz evidently required the presence of an Al-rich mineral reactant. All rocks with metamorphic Mnz also contain Ap, Ms, Bt, Pl, and Qtz. Using idealized mineral formulas, a prograde reaction that is consistent with these observations and that conserves REE in Aln and Mnz is:

$$3(CaREE)(Al_2Fe)Si_3O_{12}(OH) + Ca_5(PO_4)_3(OH) + KAl_3Si_3O_{10}(OH)_2 + 4Al_2SiO_5 + 3SiO_2$$
Aln Ap Ms And/Ky Qtz
$$= 3(REE)PO_4 + KFe_3AlSi_3O_{10}(OH)_2 + 8CaAl_2Si_2O_8 + 2H_2O.$$
Mnz Bt Pl

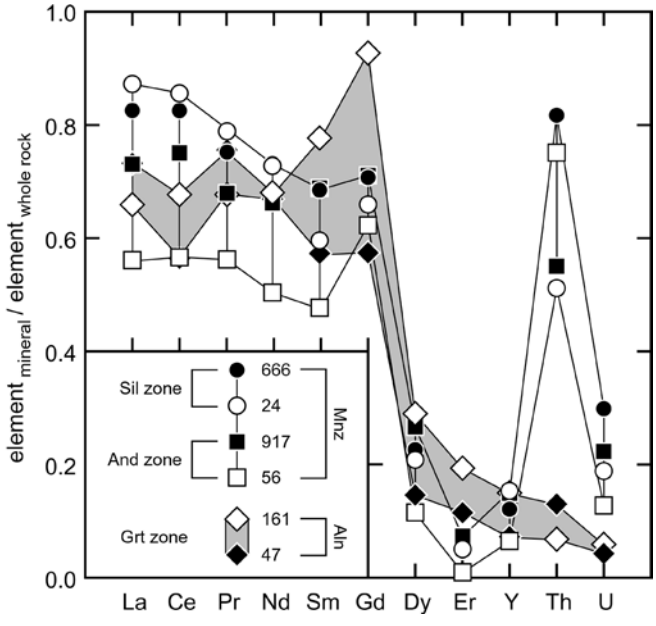

Fig. 10 Comparison between the contents of selected trace elements in whole rocks and in metamorphic monazite and allanite for representative samples of pelitic schist from the Buchan terrain, south-central Maine (cf. Tables 7, 8, 9). Almost all the LREE in each specimen are sited in allanite or monazite. The whole-rock fraction of all REE and Y is the same in allanite and monazite indicating that REE and Y were transferred locally between allanite and monazite during the allanite- and monazite-forming reactions. The much higher fractions of whole-rock Th and U contained in monazite compared to allanite indicate that a $ThSiO_4$ mineral formed with allanite during breakdown of composite monazite and then reacted with allanite to form metamorphic monazite at higher grade

In pelites, without And or Ky, St or Crd played the same role as And and Ky in the Mnz-forming reaction (with suitable adjustments of the stoichiometric coefficients). Regardless of the identity of the aluminous reactant mineral, the prograde Mnz-forming reaction also consumed a small amount of $ThSiO_4$ to account for amounts of Th in Mnz that cannot be derived from Aln (Fig. 10). The coincidence between the Mnz isograd in rocks both with and without Al-silicate and the And or Ky isograd is explained by the similar metamorphic conditions in the regional terrains at which St and And or Ky developed and the identical (or nearly so) conditions in the Buchan terrain and contact aureole at which Crd and And developed.

Monazite geochronology

$^{208}Pb/^{232}Th$ ages were measured for Mnz in 19 samples of pelitic rock (Tables 10, 11). All ages were obtained by in situ analysis of individual grains in thin section with an ion microprobe both because of the relatively small size of the grains (Fig. 5) and to document and preserve their petrographic context. Because the diameter of most Mnz grains was comparable to the diameter of the ion beam (Fig. 5), generally, only one age determination was made per grain and often the entire grain was analyzed. Rarely, two age determinations were made of the largest grains. Only Mnz grains in the matrix were measured; no grains that occur as inclusions in Grt or other minerals were analyzed. To minimize the uncertainty associated with the correction for common Pb, analyses were accepted only for those grains in which $>94\%$ of the ^{208}Pb

Table 7 REE + Y + Th + U abundance in allanite, monazite, and whole-rock garnet zone samples, Buchan terrain, south-central Maine[a]

	Sample 161 from the garnet zone with allanite					Sample 47 from the garnet zone with allanite				
	Cations in Aln (pfu)	1σ	Amount in Aln (ppm)[b]	1σ	Amount in rock (ppm)[c]	Cations in Aln (pfu)	1σ	Amount in Aln (ppm)[b]	1σ	Amount in rock (ppm)[c]
La	0.1693	0.0091	25.56	1.44	34.9	0.1292	0.0302	22.54	5.28	34.2
Ce	0.3347	0.0090	50.96	1.64	90.3	0.2628	0.0605	46.24	10.67	68.3
Pr	0.0385	0.0016	5.89	0.26	7.8	0.0306	0.0071	5.42	1.26	8.0
Nd	0.1234	0.0037	19.34	0.67	28.9	0.1033	0.0231	18.71	4.20	27.5
Sm	0.0193	0.0016	3.15	0.26	5.5	0.0177	0.0035	3.34	0.67	4.3
Gd	0.0178	0.0012	3.04	0.21	5.3	0.0169	0.0030	3.34	0.60	3.6
Dy	0.0036	0.0006	0.64	0.11	4.4	0.0055	0.0017	1.13	0.34	3.9
Y	0.0158	0.0023	1.52	0.22	21.0	0.0255	0.0107	2.85	1.20	19.0
Er	0.0016	0.0005	0.29	0.09	2.5	0.0023	0.0008	0.48	0.16	2.5
Th	0.0055	0.0018	1.38	0.44	10.6	0.0035	0.0014	1.01	0.40	14.8
U	0.0004	0.0003	0.10	0.07	2.3	0.0004	0.0003	0.12	0.09	2.1

[a]Calculations based on mineral compositions (as in Table 3), whole-rock compositions (as in Table 1), modes (Table 4), and molar volumes of minerals (Table 4), assuming an average rock density $= 2.85 \pm 0.05$ g/cm^3 from the compilation of pelite grain densities in Ague (1994)
[b]Amount of element sited in allanite or monazite
[c]Amount of element in whole rock

Table 8 REE + Y + Th + U abundance in allanite, monazite, and whole-rock andalusite zone samples, Buchan terrain, south-central Maine[a]

	Sample 56 from the andalusite zone with monazite					Sample 917 from the andalusite zone with monazite				
	Cations in Mnz (pfu)	1σ	Amount in Mnz (ppm)[b]	1σ	Amount in rock (ppm)[c]	Cations in Mnz (pfu)	1σ	Amount in Mnz (ppm)[b]	1σ	Amount in rock (ppm)[c]
La	0.1974	0.0126	24.41	2.08	43.5	0.1931	0.0213	25.64	3.01	35.1
Ce	0.4030	0.0249	50.27	4.20	88.8	0.4142	0.0248	55.48	4.02	73.9
Pr	0.0457	0.0018	5.74	0.40	10.2	0.0424	0.0013	5.71	0.30	8.4
Nd	0.1519	0.0068	19.50	1.40	38.7	0.1556	0.0066	21.46	1.26	32.4
Sm	0.0246	0.0010	3.29	0.23	6.9	0.0283	0.0015	4.06	0.27	5.9
Gd	0.0267	0.0032	3.74	0.49	6.0	0.0255	0.0011	3.84	0.23	5.4
Dy	0.0043	0.0012	0.62	0.18	5.4	0.0077	0.0004	1.20	0.08	4.5
Y	0.0213	0.0058	1.69	0.47	26.0	0.0351	0.0028	2.98	0.27	20.0
Er	0.0002	0.0002	0.03	0.03	3.0	0.0011	0.0002	0.18	0.03	2.5
Th	0.0516	0.0200	10.67	4.17	14.2	0.0318	0.0170	7.05	3.78	12.8
U	0.0017	0.0002	0.37	0.05	2.9	0.0024	0.0004	0.56	0.10	2.5

[a]Calculations based on mineral compositions (as in Table 3), whole-rock compositions (as in Table 1), modes (Table 4), and molar volumes of minerals (Table 4), assuming an average rock density $= 2.85 \pm 0.05$ g/cm^3 from the compilation of pelite grain densities in Ague (1994)
[b]Amount of element sited in allanite or monazite
[c]Amount of element in whole rock

was radiogenic (in most cases ^{208}Pb was >98% radiogenic). Between 1 and 11 grains per sample met this criterion.

Monazite was dated in 13 samples of pelitic schist from the Buchan terrain, including five with composite Mnz from the Chl and Grt zones, six with metamorphic Mnz from the And and Sil zones, and two with composite Mnz from the Sil zone (Table 10, Fig. 11). Composite Mnz from the Chl and Grt zones has a wide range of measured ages, 364–549 Ma. Ages of composite Mnz from the Sil zone span a significant although somewhat smaller range, 329–425 Ma. The ages of metamorphic Mnz from the And and Sil zones, on the other hand, are much more tightly clustered, 334–379 Ma. In spite of the whole-rock composition of sample 674 (Fig. 8), Mnz in the sample was considered composite because one of the measured ages is >400 Ma, similar to ages from other samples with composite Mnz, but completely unlike ages from samples that contain unequivocally metamorphic Mnz.

The mean square weighted deviation (MSWD) was computed for the measured Th–Pb ages from each sample to evaluate whether the Th–Pb age measurements are consistent with a single mean value. When the effect of small number statistics are taken into account, MSWD values for just three samples (663, 1002, 1014) lie within the region of 95% probability that the different age measurements for the sample are consistent with the same mean value. The upper and lower limits of the region depend on the number of samples in the set of age

Table 9 REE + Y + Th + U abundance in allanite, monazite, and whole-rock sillimanite zone samples, Buchan terrain, south-central Maine[a]

	Sample 24 from the sillimanite zone with monazite					Sample 666 from the sillimanite zone with monazite				
	Cations in Mnz (pfu)	1σ	Amount in Mnz (ppm)[b]	1σ	Amount in rock (ppm)[c]	Cations in Mnz (pfu)	1σ	Amount in Mnz (ppm)[b]	1σ	Amount in rock (ppm)[c]
La	0.1991	0.0058	24.52	2.39	28.1	0.1969	0.0100	31.70	1.95	38.4
Ce	0.4010	0.0054	49.82	4.67	58.2	0.4066	0.0189	66.03	3.85	80.0
Pr	0.0442	0.0011	5.52	0.53	7.0	0.0419	0.0019	6.84	0.39	9.1
Nd	0.1576	0.0051	20.16	1.98	27.7	0.1497	0.0014	25.02	0.91	34.2
Sm	0.0255	0.0023	3.40	0.44	5.7	0.0236	0.0025	4.11	0.46	6.0
Gd	0.0251	0.0017	3.50	0.41	5.3	0.0225	0.0020	4.10	0.39	5.8
Dy	0.0074	0.0008	1.06	0.15	5.1	0.0068	0.0007	1.29	0.14	5.7
Y	0.0390	0.0039	3.07	0.42	20.0	0.0305	0.0025	3.15	0.28	26.0
Er	0.0010	0.0003	0.14	0.05	2.8	0.0008	0.0004	0.15	0.08	3.1
Th	0.0284	0.0032	5.83	0.86	11.4	0.0377	0.0180	10.13	4.86	12.4
U	0.0021	0.0003	0.43	0.08	2.3	0.0026	0.0005	0.72	0.15	2.4

[a]Calculations based on mineral compositions (as in Table 3), whole-rock compositions (as in Table 1), modes (Table 4), and molar volumes of minerals (Table 4), assuming an average rock density $= 2.85 \pm 0.05$ g/cm^3 from the compilation of pelite grain densities in Ague (1994)
[b]Amount of element sited in allanite or monazite
[c]Amount of element in whole rock

measurements and can be determined from the 5% of sample populations that would yield a lower or higher MSWD. Probability tables of the reduced chi-square distribution in Bevington and Robinson (1992) were used to define these limits. Eight other samples give MSWD values that are much higher than the upper limit for this region. In the remaining two samples (187, 431) no MSWD was calculated because only a single Mnz grain was dated.

The mean ages of Mnz in samples 1002 and 1014 are statistically indistinguishable, and data for both samples therefore were pooled. The weighted mean age of all 14 analyzed grains in the two samples is 364.3 ± 3.5 Ma where the uncertainty is twice the standard error of the mean (SE) and MSWD = 0.99. It was anticipated that the age of Mnz in sample 663 might be different from the age of Mnz in samples 1002 and 1014 because Mnz grains in sample 663 are partially replaced by Aln that, judging from its texture, developed during retrograde metamorphism. The retrograde alteration in sample 663 may have disturbed the Th–Pb chronometer in Mnz (cf. Townsend et al. 2000). Indeed the weighted mean age of five Mnz grains in sample 663 is significantly younger than the age of Mnz in samples 1002 and 1014, 343.1 ± 9.1 Ma (± 2 SE) with MSWD = 1.01. The populations of Mnz grains in the other ten samples from the Buchan terrain either record two or more events with statistically different ages or could not be evaluated because only a single grain was dated (samples 187, 431).

Monazite was dated in four samples of pelitic schist from the Barrovian terrain, including one with composite Mnz from the Chl zone, one with metamorphic Mnz from the Ky zone, and two with composite Mnz in from the Ky zone (Table 10). Measured ages of composite Mnz from the Chl zone are 309–338 Ma. Ages of metamorphic and composite Mnz from the Ky zone are 350–359 and 335–383 Ma, respectively. Based on calculated MSWD values, only data for sample 21-28, containing metamorphic Mnz, are consistent with a single age. The weighted mean age of the population of dated Mnz grains in sample 21-28 is 352.9 ± 8.9 Ma (± 2 SE) and MSWD = 0.30.

Reliable dates of composite Mnz grains in pelites from the contact aureole could not be obtained because they all contained unacceptable concentrations of common Pb. Four grains of metamorphic Mnz were dated in each of two samples from the Sil zone (Table 10). Based in MSWD values, data for sample BME2 are consistent with a single age. The MSWD for sample ME2 lies just below the lower limit of the 95% region of probability for a single age. The simplest interpretation is that the estimated error of the individual age measurements for sample ME2 is very slightly too large. All dates for samples BME2 and ME2, therefore, were pooled. The MSWD for the combined data set (0.54) is consistent with a single weighted mean age of 403.4 ± 5.9 Ma (± 2 SE).

Discussion

Comparison of mineral distributions and reactions in New England with other studies

Results of this study confirm the conclusions of Smith and Barreiro (1990) that Aln develops from Mnz during greenschist facies regional metamorphism of pelitic schists and that metamorphic Mnz in turn develops from Aln at conditions of the lower amphibolite facies. The new data more precisely associate the Mnz-to-Aln reaction with the formation of Bt at the Bt isograd and the Aln-to-Mnz reaction with the formation of And or Ky (or St or Crd) at the And or Ky isograd. Numerous

other studies indicate that formation of metamorphic Mnz in pelites at conditions of the amphibolite facies is typical of regional metamorphism worldwide (e.g., Kingsbury et al. 1993; Lanzirotti and Hanson 1996; Foster et al. 2000; Hildebrand et al. 2001; Rubatto et al. 2001). Reports of the prograde development of Mnz from Aln at the Grt isograd in pelites from the Central Himalaya (Harrison et al. 1997; Catlos et al. 2001; Kohn et al. 2001) are difficult to compare with occurrences of Aln and Mnz in northern New England without chemical analyses of the Himalayan rocks and specific identification of the other mineral participants of the Mnz-forming reaction. The occurrence of Mnz in the chlorite zone in the three areas in New England is consistent with the observation of Mnz in very low grade metamorphic rocks elsewhere (e.g., Franz et al. 1996; Heinrich et al. 1997; Rasmussen et al. 2001, 2002; Rubatto et al. 2001). The instability of Mnz reported for one instance of weathering (Sawka et al. 1986) cannot be a general phenomenon because there are numerous unequivocal examples of detrital Mnz in greenschist and amphibolite facies metamorphic rocks (e.g., Suzuki and Adachi 1994; Suzuki et al. 1994; Catlos et al. 2001; Rubatto et al. 2001; Rasmussen et al. 2002; this study, as discussed below).

Unlike the case of Mnz, the occurrence of prograde metamorphic Aln in pelitic schists has not been widely noted in recent investigations. The absence of Aln in pelites studied by Franz et al. (1996), Heinrich et al. (1997), and Rubatto et al. (2001) can be attributed to the lack of samples collected from appropriate portions of the metamorphic terrain (i.e., Bt and Grt zones). The absence of Aln and presence of Mnz in the greenschist facies of the Wepawaug Formation (Lanzirotti and Hanson 1996) can be explained by the relatively low Ca contents of Wepawaug pelites (Ague 1994) and the dependence of the development of Aln on whole-rock chemical composition (Fig. 7). Likewise the absence of Aln in two samples of pelite from the Bt zone examined by Kinsgbury et al. (1993) can be explained by the rocks' low Ca contents. The occurrence of LREE oxides and phosphates, rather than Mnz in the greenschist facies rocks examined by Kingsbury et al. (1993), however, is puzzling. Textures of the REE phases from the greenschist facies illustrated in Kingsbury et al. (1993) suggest that Mnz might have been stable at the peak of metamorphism, but was later consumed by retrograde reactions as has been documented elsewhere (e.g., Pan 1997; Bea 1999).

Reactions proposed by others to explain the formation of Mnz have also involved participation of major minerals. The reaction suggested by Simpson et al. (2000) is nearly identical to the Mnz-forming reaction inferred in this study. Bingen et al. (1996) proposed a linked development of prograde metamorphic Mnz and minerals produced by the hornblende-to-clinopyroxene reaction at the transition from the amphibolite to the granulite facies in metamorphosed calc-alkaline igneous rocks. The unusually high grade of the Mnz-forming reaction (compared with that in pelitic rocks) may reflect the control of bulk rock composition both on the conditions and on the mineral reactants and products of the Mnz-forming reaction.

The difference in texture observed in this study between low-grade Mnz with xenoblastic forms and high-grade Mnz with idioblastic forms (Fig. 5) has also been reported from suites of progressively metamorphosed pelitic rocks elsewhere (e.g., Franz et al. 1996; Rubatto et al. 2001).

Origin and significance of composite monazite

Rasmussen et al. (2002) describe Mnz from low-grade metamorphosed pelitic rocks from Australia that is texturally identical to composite Mnz from the Chl and Grt zones of the Waterville Formation in the Buchan terrain. In both cases the Mnz has an inclusion free core that contrasts in BSE brightness with an inclusion-rich rim. The Mnz grains from Australia are large enough that Rasmussen et al. (2002) obtained separate ion microprobe dates of core and rim. Rims had ages consistent with growth during regional metamorphism. Cores had ages up to 240 Ma older than the rims and were considered detrital. Composite grains from the Waterville Formation are too small to permit separate dating of core and rim by ion microprobe analysis (Fig. 5A). Nevertheless, the range of dates obtained for all analyzed composite Mnz grains from the Chl zone indicate the presence of age domains like those in the Australian Mnz. The two oldest dates of Mnz from the Chl zone are older than the sedimentation age of the host Waterville Formation (Fig. 11). The two youngest dates are within the range of ages of metamorphic Mnz from the And and Sil zones. Most measured ages of low-grade composite Mnz lie between these extremes. On the basis of the its measured ages (Fig. 11) and its textural similarity to the Australian Mnz, low-grade composite Mnz from the Waterville Formation is considered composed of a detrital core surrounded by a rim that grew during Acadian regional metamorphism. The range of ages obtained for the low-grade composite Mnz (Tables 10, 11, Fig. 11) would result from analysis of small grains in which both core and rim were positioned under the ion beam in different proportions in different grains. The occurrence of detrital Mnz or Mnz grains with a detrital component is not uncommon in pelitic schists from the greenschist and amphibolite facies worldwide (e.g., Suzuki and Adachi 1994; Suzuki et al. 1994; Catlos et al. 2001; Rubatto et al. 2001). Composite Mnz grains from the Barrovian terrain and the contact aureole therefore likely have the same origin as composite Mnz in the Buchan terrain although supporting evidence from ion microprobe dating is lacking.

Any attempt to determine the age of metamorphism by dating Mnz in pelitic rocks must consider the difference between composite and metamorphic Mnz,

Table 10 Measured Th–Pbages of monazite grains. Buchan terrain, south-central Maine

Terrain	Sample	Grain	Zone	Mnz type[a]	Age[b] (Ma)	$1\sigma_{age}$[c] (Ma)	$^{208}Pb^{*}$[d] (%)
Buchan	56	1	And	M	369.1	6.3	98.0
Buchan	56	2	And	M	344.0	5.8	96.5
Buchan	56	3	And	M	357.9	6.1	96.2
Buchan	56	4	And	M	367.9	6.3	98.6
Buchan	56	5	And	M	375.0	6.4	96.2
Buchan	56	6	And	M	359.8	6.1	95.9
Buchan	56	7	And	M	347.9	5.9	97.4
Buchan	1002	1	And	M	360.6	6.1	96.7
Buchan	1002	2	And	M	365.5	6.2	98.6
Buchan	1002	3	And	M	358.6	6.1	98.4
Buchan	1002	4	And	M	363.0	6.2	98.0
Buchan	1002	5	And	M	369.3	6.3	98.5
Buchan	1002	6	And	M	362.4	6.2	94.6
Buchan	1002	7	And	M	368.0	6.3	97.8
Buchan	662	1	Sil	M	357.2	6.1	96.9
Buchan	662	2	Sil	M	360.7	6.1	97.7
Buchan	662	3	Sil	M	368.5	6.3	98.7
Buchan	662	4	Sil	M	334.4	5.7	99.7
Buchan	905	1	Sil	M	353.4	6.0	99.0
Buchan	905	2	Sil	M	363.7	6.2	99.4
Buchan	905	3	Sil	M	354.2	6.0	98.0
Buchan	905	4	Sil	M	378.7	6.4	95.4
Buchan	1014	1	Sil	M	366.4	6.2	99.6
Buchan	1014	2	Sil	M	367.1	6.2	99.6
Buchan	1014	3	Sil	M	367.6	6.2	97.5
Buchan	1014	4	Sil	M	364.0	6.2	97.1
Buchan	1014	5	Sil	M	375.2	6.4	98.5
Buchan	1014	6	Sil	M	348.8	5.9	99.1
Buchan	1014	7	Sil	M	366.3	6.2	97.5
Buchan	411	1	Chl	C	369.6	6.3	97.5
Buchan	411	1	Chl	C	409.8	7.0	94.4
Buchan	411	2	Chl	C	363.7	6.2	97.2
Buchan	411	3	Chl	C	378.5	6.4	98.0
Buchan	417	1	Chl	C	549.1	9.3	97.8
Buchan	417	2	Chl	C	486.2	8.3	98.3
Buchan	417	3	Chl	C	453.5	7.7	97.4
Buchan	431	1	Chl	C	391.8	6.7	96.8
Buchan	53	1	Grt	C	370.1	6.3	94.8
Buchan	53	2	Grt	C	372.4	6.3	98.4
Buchan	53	3	Grt	C	390.6	6.6	97.9
Buchan	53	3	Grt	C	393.3	6.7	98.1
Buchan	53	4	Grt	C	385.7	6.6	97.7
Buchan	53	5	Grt	C	392.8	6.6	97.2
Buchan	187	1	Grt	C	403.1	6.9	95.1
Buchan	674	1	Sil	C	425.0	7.2	95.2
Buchan	674	2	Sil	C	338.5	5.8	99.6
Buchan	674	2	Sil	C	359.4	6.1	99.6
Buchan	674	3	Sil	C	333.3	5.7	99.2
Buchan	674	4	Sil	C	361.6	6.1	98.5
Buchan	674	5	Sil	C	358.7	6.1	98.8
Buchan	674	6	Sil	C	360.8	6.1	99.0
Buchan	674	7	Sil	C	329.3	5.6	99.6
Buchan	674	8	Sil	C	331.7	5.6	99.5
Buchan	969	1	Sil	C	381.3	6.5	97.8
Buchan	969	2	Sil	C	380.6	6.5	98.8
Buchan	969	3	Sil	C	375.8	6.4	99.0
Buchan	663	1	Sil	MR	342.8	5.8	98.5
Buchan	663	2	Sil	MR	334.3	5.7	99.1
Buchan	663	3	Sil	MR	342.2	5.8	99.0
Buchan	663	4	Sil	MR	349.4	5.9	99.5
Buchan	663	5	Sil	MR	347.3	5.9	93.8

[a] Analyzed monazite is composite (*C*), metamorphic (*M*), or metamorphic partially altered to retrograde allanite (*MR*). See text for details

[b] See text for details of measurement

[c] 1σ uncertainty on each Th–Pbage calculated from the relative pooled standard deviation of age measurements on monazite standard 554 (1.7% of the mean)

[d] % radiogenic ^{208}Pb in the monazite grain is $[1-(^{208}Pb/^{204}Pb)_{initial}/(^{208}Pb/^{204}Pb)_{measured}]$ x100% based on an assumed value of 36.7 for $(^{208}Pb/^{204}Pb)_{initial}$

particularly in investigations that specifically target Mnz inclusions in Grt for radiometric dating (e.g., Foster et al. 2000; Stern and Berman 2000; Catlos et al. 2001; Bell and Welch 2002). Composite Mnz will not be replaced by metamorphic Aln at conditions of the Bt isograd in rocks with below-average Ca and/or

Table 11 Measured Th–Pb ages of monazite grains. Barrovian terrain, east-central Vermont, and contact aureole, central Maine

Terrain	Sample	Grain	Zone	Mnz type[a]	Age[b] (Ma)	$1\sigma_{age}$[c] (Ma)	$^{208}Pb^{*}$[d] (%)
Barrovian	21-28	1	Ky	M	358.7	6.1	99.0
Barrovian	21-28	2	Ky	M	351.3	6.0	99.4
Barrovian	21-28	3	Ky	M	351.9	6.0	98.2
Barrovian	21-28	3	Ky	M	352.8	6.0	99.4
Barrovian	21-28	4	Ky	M	350.2	6.0	99.5
Barrovian	NHd1O	1	Chl	C	333.7	5.7	98.5
Barrovian	NHd1O	2	Chl	C	337.5	5.7	97.2
Barrovian	NHd1O	3	Chl	C	324.0	5.5	99.2
Barrovian	NHd1O	4	Chl	C	308.5	5.2	99.1
Barrovian	NHd1O	5	Chl	C	337.4	5.7	98.4
Barrovian	NHd1O	6	Chl	C	315.4	5.4	97.9
Barrovian	NHd1O	6	Chl	C	328.4	5.6	96.5
Barrovian	21-25A	1	Ky	C	348.0	5.9	97.7
Barrovian	21-25A	2	Ky	C	335.2	5.7	98.5
Barrovian	21-25A	3	Ky	C	344.4	5.9	98.0
Barrovian	21–25A	4	Ky	C	337.1	5.7	97.0
Barrovian	21-25A	5	Ky	C	343.3	5.8	96.4
Barrovian	21-25A	6	Ky	C	336.9	5.7	96.9
Barrovian	21-25A	7	Ky	C	358.3	5.9	99.1
Barrovian	21-25A	8	Ky	C	382.7	5.7	97.8
Barrovian	21-25A	9	Ky	C	361.0	5.8	99.0
Barrovian	21-25A	10	Ky	C	352.2	5.7	96.8
Barrovian	21-25A	11	Ky	C	358.5	6.1	98.5
Barrovian	21-29G	1	Ky	C	346.9	5.9	99.2
Barrovian	21-29G	2	Ky	C	359.4	6.1	99.2
Barrovian	21-29G	3	Ky	C	351.3	6.0	99.1
Barrovian	21-29G	4	Ky	C	358.5	6.1	98.6
Barrovian	21-29G	4	Ky	C	351.0	6.0	98.3
Barrovian	21-29G	6	Ky	C	347.4	5.9	96.7
Barrovian	21-29G	7	Ky	C	365.7	5.9	98.5
Barrovian	21-29G	8	Ky	C	366.8	6.2	99.0
Aureole	BME2[e]	1	And	M	407.6	6.9	98.3
Aureole	BME2[e]	2	And	M	399.9	6.8	98.7
Aureole	BME2[e]	3	And	M	407.6	6.9	97.6
Aureole	BME2[e]	3	And	M	412.4	7.0	95.5
Aureole	ME2	1	Sil	M	400.9	6.8	95.3
Aureole	ME2	2	Sil	M	397.3	6.8	99.7
Aureole	ME2	3	Sil	M	401.3	6.8	99.2
Aureole	ME2	4	Sil	M	401.4	6.8	98.8

[a]Analyzed monazite is composite (*C*), metamorphic (*M*). See text for details

[b]See text for details of measurement

[c]1σ uncertainty on each Th–Pbage calculated from the relative pooled standard deviation of age measurements on monazite standard 554 (1.7% of the mean)

[d]%radiogenic ^{208}Pb in the monazite grain is $[1-(^{208}Pb/^{204}Pb)_{initial}/(^{208}Pb/^{204}Pb)_{measured}]\times 100$-%based on an assumed value of 36.7 for $(^{208}Pb/^{204}Pb)_{initial}$

[e]SampleBME2 was collected from the contact aureole at the northeast margin of the pluton outside Fig. 3

Al contents (Fig. 7). The composite Mnz then is available to be trapped as inclusions in Grt that grows under conditions of the Grt zone. (Allanite will develop at the expense of composite Mnz at the Bt isograd in pelites with average or above-average Ca and/or Al contents. In these rocks, Aln rather than Mnz, therefore, will be trapped as inclusions in Grt that grows in the Grt zone.) The measured age of composite Mnz, either as inclusions in Grt or in the matrix, will only provide an upper bound on the age of the metamorphic event rather than the age of a discreet crystallization event. Fortunately, with sufficient sampling, composite Mnz can be distinguished from metamorphic Mnz in a number of ways, including mineral chemistry (Fig. 6) and whole-rock chemistry (Fig. 7). In addition, matrix Mnz from the And or Ky zone or from higher grades likely is metamorphic rather than composite if equivalent lower grade rocks in the greenschist facies contain Aln but not Mnz (as in the contact aureole, Fig. 3). If rocks that contain Grt porphyroblasts with Aln inclusions have Mnz in the matrix, the Mnz is almost certainly metamorphic rather than composite. On the other hand, matrix Mnz could be composite in rocks that contain Grt porphyroblasts with Mnz inclusions.

Interpretation of measured ages of monazite

Factors that determine measured monazite ages in pelitic schists

Five different processes were considered in the interpretation of measured ages of Mnz grains in pelitic schists from New England. The first is incorporation of detrital Mnz into the sedimentary protolith of the pelites. If detrital Mnz forms the core of a grain, the measured age of that grain only provides an upper bound on the age of metamorphism.

Second, detrital Mnz grains were transformed into composite grains following growth of a rim during very

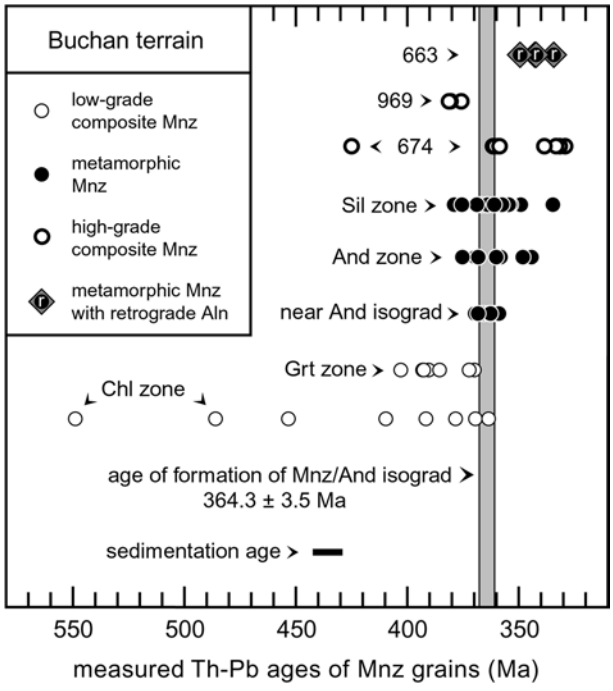

Fig. 11 Summary of age measurements of monazite in pelitic schists from the Waterville Formation in the Buchan terrain, south-central Maine. Each *symbol* represents one age determination (see Table 10 for all data). *Vertical gray bar* represents the preferred estimate of the age of peak metamorphism at the andalusite isograd based on data for samples 1002 and 1014 (see text). Sedimentation age from Tucker et al. (2001). Age of several composite monazite grains from the Chl zone >450 Ma prove that they have a detrital component. The more restricted range in age of composite Mnz grains from the garnet zone suggests that they were partially recrystallized during regional metamorphism. The spread in ages for metamorphic monazite grains from the andalusite and sillimanite zones as well as the measured ages for monazite in samples 663, 674, and 969 specifically discussed in text

low-grade metamorphism (grade much lower than the Bt isograd) by a yet unknown heterogeneous mineral reaction. Analysis of the rim, separate from the core, may yield the age of low-grade metamorphism (e.g., Rasmussen et al. 2002). Analysis of composite Mnz grains about the same size as the ion beam, however, will yield an age intermediate between the age at which the detrital core formed and the time of metamorphism.

A third process emerges from the observation that the range of measured ages for composite Mnz from the Grt zone of the Buchan terrain is much narrower and on average closer to the measured age of metamorphic Mnz than the range of ages for composite Mnz from the Chl zone (Fig. 11). The differences cannot be explained by thicker rims on composite Mnz grains from the Grt zone because composite Mnz from the Grt zone has about the same size as composite Mnz from the Chl zone. The differences imply that composite Mnz recrystallized during prograde metamorphism in the Grt zone and at higher grades even in the absence of the mineral's obvious participation in heterogeneous mineral reactions. If recrystallization did not go to completion during metamorphism, measured ages of whole single composite Mnz grains will be intermediate between the age of the original detrital core and the age of the metamorphic event, but closer to the age of metamorphism than the measured ages of unrecrystallized composite grains.

A fourth process is the formation of metamorphic Mnz neoblasts at conditions of the And or Ky isograds by heterogeneous reactions involving Aln and other minerals in pelitic rocks.

If the Mnz neoblasts can be identified on the basis of texture (Fig. 5), mineral chemistry (Fig. 6), and/or whole-rock chemistry (Figs. 7 and 8) and if they have compositions unmodified by later retrograde metamorphism, their measured ages date not just the metamorphic event, but more specifically the formation of Al-silicate at the And and Ky isograds.

Fifth, several samples of pelitic schist from the And and Sil zones of the Buchan terrain contain Mnz with rims of Aln that are interpreted as a product of retrograde metamorphism. Retrograde mineral-fluid reactions may partially or completely reset the Mnz Th–Pb chronometer in individual grains (e.g., Townsend et al. 2000). Measured ages of Mnz grains altered during retrograde metamorphism place a lower bound on the age of peak metamorphism.

Assessment of the diffusive loss of Pb from metamorphic Mnz crystals is complicated by conflicting results from both laboratory diffusion experiments and geochronological studies of Mnz in metamorphic rocks. Values of the activation energy for Pb diffusion in Mnz derived from the experimental data of Smith and Giletti (1997), and of Cherniak (2000) and Cherniak et al. (2000), differ by a factor of about three. Results of Cherniak (2000) and Cherniak et al. (2000) imply a very high closure T (Dodson 1973) for Mnz during metamorphism whereas results of Smith and Giletti (1997) imply a significantly lower closure T. A number of geochronological studies of Mnz in metamorphic rocks suggest that the retention of Pb in Mnz is probably intermediate between that predicted by the two sets of experimental data (Copeland et al. 1988; Suzuki et al. 1994; Spear and Parrish 1996; Grove and Harrison 1999). Considerations of the ionic porosity of Mnz (Dahl 1997) are also consistent with an activation energy for Pb diffusion in Mnz that is larger than that derived from the data of Smith and Giletti (1997). The large discrepancies among the various studies is not fully understood, but may mean that data for Pb diffusion in Mnz at high T cannot be extrapolated linearly to low T using conventional methods.

In any case, the data of Grove and Harrison (1999) suggest a Pb diffusivity in Mnz at 650 °C of $\approx 10^{-28}$ m^2 s^{-1}. Regardless of the activation energy, these data imply that Pb loss from Mnz under the full range of amphibolite facies conditions for ten's of millions of years typically does not exceed a few percent for the grain sizes (20–30 μm) considered in this study. Indeed, numerous other studies have argued that there is limited Pb loss by volume diffusion from Mnz in metamorphic rocks during cooling from amphibolite facies conditions (e.g., Parrish 1990; Smith and Barreiro 1990; Getty and

Gromet 1992; Kingsbury et al. 1993; Hawkins and Bowring 1997; Cocherie et al. 1998; Crowley and Ghent 1999; Foster et al. 2000; Krohe and Wawrzenitz 2000; Catlos et al. 2001; Rubatto et al. 2001). Significant diffusive Pb loss from Mnz in the Buchan terrain of this study can be ruled out because measured Mnz ages do not decrease with increasing metamorphic grade (Fig. 11). The age of metamorphic Mnz formed in sample 1002 at the And isograd is indistinguishable from the age of metamorphic Mnz in sample 1014 from the highest-grade portion of the terrain in the Sil zone (Fig. 1, Tables 10, 11). Thus, Pb loss by diffusion from Mnz grains was not considered in the interpretation of their measured ages.

Buchan terrain, south-central Maine

Measured ages of the pooled population of analyzed metamorphic Mnz grains in samples 1002 and 1014 (Tables 10, 11) are consistent with a single weighted mean age of 364.3 ± 3.5 Ma (± 2 SE). Interpretation of the age is uncomplicated by considerations of possible detrital cores and low-grade overgrowths. There is no mineralogical or geochronological evidence that Mnz ages in the two samples were disturbed by retrograde metamorphism. The concordant 367 ± 1 Ma U–Pb date for Mnz and Zrn from an undeformed pegmatite at Gardiner, 9 km south of the southern boundary of the area in Fig. 1 (Tucker et al. 2001), records high-grade post-kinematic regional metamorphism at an age within error of measurement of the ages of Mnz in samples 1002 and 1014. The mean age of metamorphic Mnz grains in the two samples, therefore, is considered to date the formation of And at the And isograd at the peak of Buchan metamorphism.

The age is significantly younger than Rb–Sr whole-rock ages (385–395 Ma, Dallmeyer and van Breeman 1981) or U–Pb Zrn and Spn ages (378–381 Ma, Tucker et al. 2001) of granite plutons that intrude the area within and near Fig. 1. If the peak of metamorphism in the Buchan terrain was synchronous with emplacement of the plutons, the mean Mnz age for samples 1002 and 1014 must record a post-peak episode of retrograde metamorphism. The possibility, however, appears unlikely. The coincidence of the Mnz and the And isograds demonstrate that formation of Mnz in the samples was a peak prograde metamorphic phenomenon rather than the product of later retrograde metamorphism. Metamorphic Mnz grains that have ages disturbed by the episode of retrograde metamorphism in the Buchan terrain either show mineralogical evidence for alteration (such the Aln rims on metamorphic Mnz in sample 663), or record a range of ages between ≈364 and ≈343 Ma (such samples 56, 662, and 905). Samples 1002 and 1014 do neither. The peak of regional metamorphism in the Buchan terrain appears to have been later than intrusion of the plutons in the area of Fig. 1.

A peak of regional metamorphism that followed emplacement of the granite plutons in the Buchan terrain is consistent with a variety of structural and petrologic observations summarized by Osberg (1988): (1) Granites display a mortar texture and contain Bt–Grt pairs that record metamorphic rather than magmatic T (see also Ferry 1978); (2) isograds in pelitic schists can be traced through the plutons on the basis of the minerals observed in xenoliths; and (3) mats of Sil are developed parallel to the axial planes of late folds that deform granite dikes associated with the plutons. A younger age of peak metamorphism relative to granite emplacement is also consistent with the cooling history of the plutons deduced by Dallmeyer and van Breeman (1981) from $^{40}Ar/^{39}Ar$ ages of minerals from the granites and other information. They concluded that the plutons cooled rapidly from ≈650 °C after emplacement at 380–390 Ma and then resided at the T of peak metamorphism for a protracted period at ≈350 Ma before continued rapid cooling beginning before ≈330 Ma. The close spatial association between isograds mapped in metacarbonate rocks and the locations of the plutons in Fig. 1 (Ferry 1976, 1983) either is a coincidence or indicates that index minerals in the carbonate rocks developed during ≈380-Ma contact metamorphism and were then preserved through the peak of regional metamorphism that followed ≈15 Ma later.

Measured Th–Pb dates of Mnz grains in a third sample, 663, are also consistent with a single mean age, 343.1 ± 9.1 Ma (± 2 SE). The age is significantly younger than the inferred age of peak metamorphism. The petrographic feature that distinguishes sample 663 from samples 1002 and 1014 is the partial replacement of metamorphic Mnz by retrograde Aln. The mean age of Mnz in sample 663, therefore, is tentatively interpreted as the age of an episode of retrograde metamorphism. What exactly the episode of retrograde metamorphism corresponds to in a broader consideration of the geologic history of the Buchan terrain is unknown. The remaining three analyzed samples with metamorphic Mnz (samples 56, 662, 905, Tables 10, 11) contain populations of grains whose ages are statistically inconsistent with a single value. The measured age of each individual grain in the three samples is within error of either the inferred age of peak metamorphism (364.3 ± 3.5 Ma) or the inferred age of the episode of retrograde metamorphism (343.1 ± 9.1 Ma). Monazite grains in samples 56, 662, and 905 likely are composed of subgrain age domains developed at the peak of prograde metamorphism and during retrograde metamorphism. The range of measured ages in each sample would result from analyses of small grains in which both types of domains were positioned under the ion beam in different proportions. Measured ages close to ≈364 Ma likely were obtained from portions of grains mostly or entirely formed at the peak of metamorphism. Measured ages close to ≈343 Ma likely were obtained mostly or entirely from material recrystallized during the episode of retrograde metamorphism.

None of the analyzed samples with composite Mnz contains a population of grains consistent with a single age. The range of ages of composite Mnz grains in samples from the Chl zone (Fig. 11, Tables 10, 11) is believed to result from analyzing a mixture of subgrain age domains corresponding to an unrecrystallized (or largely unrecrystallized) detrital Mnz core and a rim that grew during very low-grade metamorphism. The oldest age of Mnz from the Chl zone (549.1 ± 18.6 Ma, $\pm 2\sigma$, sample 417) then represents a minimum age of formation of the detrital Mnz. The youngest age (363.7 ± 12.4 Ma, $\pm 2\ \sigma$, sample 411) is within error of the inferred age of peak regional metamorphism, 364.3 ± 3.5 Ma.

Measured ages of individual composite Mnz grains in samples 53, 187, 674, and 969 from the Grt and Sil zones may be either significantly older than, the same within error of, or significantly younger than the inferred age of peak metamorphism (Fig. 11, Tables 10, 11). Ages of composite Mnz in the four samples are tentatively interpreted as the result of analyzing mixtures in different proportions of subgrain age domains consisting of unrecrystallized detrital Mnz, detrital material recrystallized during prograde metamorphism, a rim that grew during low-grade regional metamorphism, and Mnz recrystallized during retrograde metamorphism. Partial recrystallization of the detrital material explains the narrower range of measured ages in samples 53, 187, 674, and 969 compared with the range of ages in samples from the Chl zone. The oldest measured ages for Mnz in samples 53, 187, 674, and 969 are likely derived from analysis of grains that retain a significant unrecrystallized detrital component. The youngest ages are likely derived from analysis of grains that have a large component of Mnz recrystallized during retrograde metamorphism. Measured ages that are within the range of the inferred age of peak metamorphism are derived either from analysis of Mnz primarily grown or recrystallized during peak metamorphism, or from analysis of a fortuitous combination of detrital Mnz, retrograde Mnz, and Mnz recrystallized during peak metamorphism.

The range of ages measured for composite Mnz in samples 674 and 969, and for metamorphic Mnz in samples 56, 662, and 905 are interpreted in terms of age domains within individual grains. The interpretation is supported by the very common occurrence of age domains in Mnz crystals from pelitic schists worldwide (e.g., DeWolf et al. 1993; Hawkins and Bowring 1997; Cocherie et al. 1998; Crowley and Ghent 1999; Townsend et al. 2000; Rubatto et al. 2001; Rasmussen et al. 2002). Unfortunately there is no independent textural evidence for age domains. Monazite grains from the five samples all appear nearly featureless in BSE imaging, similar to the grain in illustrated in Fig. 5D. The absence of independent textural evidence, however, is not a fatal shortcoming of the interpretation. Chemical domains within Mnz grains displayed by contrasts in BSE brightness do not necessarily correspond to age domains, and age domains do not always display significant contrast in BSE brightness (Crowley and Ghent 1999).

Barrovian terrain, east-central Vermont

Dates for the population of metamorphic Mnz grains in sample 21-28 (Tables 10, 11) are consistent with a single weighted mean age of 352.9 ± 8.9 Ma (± 2 SE). None of the Mnz grains in sample 21-28 show petrographic evidence for retrograde alteration. Spear and Harrison (1989) reported a range of $^{40}Ar/^{39}Ar$ ages of four samples of metamorphic Hbl from the Standing Pond volcanics near the area of Fig. 2, 350–397 Ma, that encompasses the weighted mean age of metamorphic Mnz in sample 21-28. The mean age of Mnz in sample 21-28, therefore, is considered to date the formation of Ky at the Ky isograd during the peak of Barrovian regional metamorphism.

The other three analyzed samples from the Barrovian terrain contain composite Mnz (Tables 10, 11). The population of measured Mnz ages in none of the three samples is consistent with a single age. As with composite Mnz from the Buchan terrain, the ages are tentatively interpreted as the result of analyzing mixtures of subgrain age domains that correspond to an unrecrystallized detrital Mnz core, a rim that grew during low-grade regional metamorphism, detrital material recrystallized during prograde metamorphism, and Mnz recrystallized during retrograde metamorphism. Individual measured ages may be either significantly older than or significantly younger than the inferred age of peak metamorphism (Tables 10, 11). The older ages are likely derived from analysis of material that retains a significant unrecrystallized detrital component. The younger ages are likely derived from analysis of material that has a significant component of Mnz recrystallized during retrograde metamorphism. Ages of composite Mnz grains that are within the range of the inferred age of peak metamorphism are derived from analysis either of Mnz primarily grown or recrystallized during peak metamorphism, or of a fortuitous combination of detrital Mnz, retrograde Mnz, and Mnz recrystallized during peak metamorphism.

Contact aureole, central Maine

Dates for the analyzed population of metamorphic Mnz from the contact aureole are consistent with a single mean age of 403.4 ± 5.9 Ma (± 2 SE). There is no petrographic evidence for retrograde alteration of the metamorphic Mnz. Concordant U–Pb ages of Zrn from the intrusion are 405 ± 3 Ma (Bradley et al. 2000). The age of metamorphic Mnz dates the intrusion of the pluton and the formation of And at the And isograd during the associated episode of contact metamorphism.

Acknowledgments J.M.F. and B.A.W. thank Liz Catlos and especially Chris Coath for instructing us in the use of the UCLA ion microprobe and assisting with the interpretation of results. Ken Livi designed the protocol for electron microprobe analysis of monazites and allanites. We benefited from discussions of ion microprobe analysis, age relations in northern New England, and closure temperature in monazite with Jack Cheney, Chris Hepburn, Frank Spear, Bob Tucker, and Bruce Watson. We thank David Hawkins and Frank Spear for thorough and thoughtful critical reviews. Research supported by grant EAR-9805346 from the Division of Earth Sciences, National Science Foundation. The ion microprobe facility at UCLA is partly supported by a grant from the Instrumentation and Facilities Program, Division of Earth Sciences, National Science Foundation.

References

Ague JJ (1994) Mass transfer during Barrovian metamorphism of pelites, south-central Connecticut. I: evidence for changes in composition and volume. Am J Sci 294:989–1057

Armstrong JT (1988) Quantitative analysis of silicate and oxide minerals: comparison of Monte Carlo, ZAF and phi–rho-z procedures. In: Newbury DE (ed) Microbeam analysis, 1988. San Francisco Press, San Francisco, pp 239–246

Barnett DE, Chamberlain CP (1991) Relative scales of thermal- and fluid infiltration-driven metamorphism in fold nappes, New England, USA. Am Mineral 76:713–727

Bea F, Montero P (1999) Behavior of accessory phases and redistribution of Zr, REE, Y, Th, and U during metamorphism and partial melting of metapelites in the lower crust: an example from the Kinzigite Formation of Ivrea-Verbano, NW Italy. Geochim Cosmochim Acta 63:1133–1153

Bell TH, Welch PW (2002) Prolonged Acadian orogenesis: revelations from foliation intersection axis (FIA) controlled monazite dating of foliations in porphyroblasts and matrix. Am J Sci 302:549–581

Bevington PR, Robinson DK (1992) Data reduction and error analysis for the physical sciences. WCB/McGraw-Hill, Boston

Bingen B, Demaiffe D, Hertogen J (1996) Redistribution of rare earth elements, thorium, and uranium over accessory minerals in the course of amphibolite to granulite facies metamorphism: the role of apatite and monazite in orthogneisses from southwestern Norway. Geochim Cosmochim Acta 60:1341–1354

Bradley DC, Tucker RD, Lux DR, Harris AG, McGregor DC (2000) Migration of the Acadian orogen and foreland basin across the northern Appalachians of Maine and adjacent areas. US Geol Surv Prof Paper 1624

Catlos EJ, Harrison TM, Kohn MJ, Grove M, Ryerson FJ, Manning CE, Upreti BN (2001) Geochronologic and thermobarometric constraints on the evolution of the Main Central Thrust, central Nepal Himalaya. J Geophys Res 106:16177–16204

Cherniak DJ (2000) Diffusion in accessory minerals—a progress report. Eleventh Annual V. M. Goldschmidt Conference, Abstract #3239. LPI Contribution No. 1088, Lunar and Planetary Institute, Houston (CD-ROM)

Cherniak DJ, Watson EB, Harrison TM, Grove M (2000) Pb diffusion in monazite: a progress report on a combined RBS/SIMS study. Trans Am Geophys Union 81:S25.

Cocherie A, Legendre O, Peucat JJ, Kouamelan AN (1998) Geochronology of polygenetic monazites constrained by in situ electron microprobe Th–U–total Pb determination: implications for lead behaviour in monazite. Geochim Cosmochim Acta 62:2475–2497

Copeland P, Parrish RR, Harrison TM (1988)Identification of inherited radiogenic Pb in monazite and its implications for U–Pb systematics. Nature 333:760–763

Crowley JL, Ghent ED (1999) An electron microprobe study of the U–Th–Pb systematics of metamorphosed monazite: the role of Pb diffusion versus overgrowth and recrystallization. Chem Geol 157:285–302

Dahl PS (1997) A crystal–chemical basis for Pb retention and fission-track annealing systematics in U-bearing minerals, with implications for geochronology. Earth Planet Sci Lett 150:277–290.

Dallmeyer RD, van Breeman O (1981) Rb–Sr whole-rock and $^{40}Ar/^{39}Ar$ ages of the Togus and Hallowell quartz monzonite and Three Mile Pond granodiorite plutons, south-central Maine: their bearing on post-Acadina cooling history. Contrib Mineral Petrol 78:61–73

DeWolf CP, Belshaw N, O'Nions RK (1993) A metamorphic history from micron-scale $^{207}Pb/^{206}Pb$ chronometry of Archean monazite. Earth Planet Sci Lett 120:207–220

Dodson M (1973) Closure temperature in cooling geochronological and petrological systems. Contrib Mineral Petrol 40:259–274

Doll CG, Cady WM, Thompson JB Jr, Billings MP, compilers and editors (1961) Centennial Geologic Map of Vermont. Vermont Geologic Survey, Montpelier, Vermont

Dollase WA (1971) Refinement of the crystal structure of epidote, allanite, and hancockite. Am Mineral 56:447–464

Ferry JM (1976) Metamorphism of calcareous sediments in the Waterville–Vassalboro area, south-central Maine: mineral reactions and graphical analysis. Am J Sci 276:841–882

Ferry JM (1978) Fluid interaction between granite and sediment during metamorphism, south-central Maine. Am J Sci 278:1025–1056

Ferry JM (1980) A comparative study of geothermometers and geobarometers in pelitic schists from south-central Maine. Am Mineral 65:720–732

Ferry JM (1981) Petrology of graphitic sulfide-rich schists from south-central Maine: an example of desulfidation during prograde regional metamorphism. Am Mineral 66:908–930

Ferry JM (1982) A comparative geochemical study of pelitic schists and metamorphosed carbonate rocks from south-central Maine, USA. Contrib Mineral Petrol 80:59–72

Ferry JM (1983) Regional metamorphism of the Vassalboro Formation, south-central Maine, USA: a case study of the role of fluid in metamorphic petrogenesis. J Geol Soc Lond 140:551–576

Ferry JM (1984) A biotite isograd in south-central Maine, USA: mineral reactions, fluid transfer, and heat transfer. J Petrol 25:871–893

Ferry JM (1987) Metamorphic hydrology at 13-km depth and 400–550 °C. Am Mineral 72:39–58

Ferry JM (1988) Infiltration-driven metamorphism in northern New England, USA. J Petrol 29:1121–1159

Ferry JM (1994) Overview of the petrologic record of fluid flow during regional metamorphism in northern New England. Am J Sci 294:905–988

Finger F, Broska I, Roberts MP, Schermaier A (1998) Replacement of primary monazite by apatite–allanite–epidote coronas in an amphibolite facies granite gneiss from the eastern Alps. Am Mineral 83:248–258

Foster G, Kinny P, Vance D, Prince C, Harris N (2000) The significance of monazite U–Th–Pb age data in metamorphic assemblages; a combined study of monazite and garnet chronometry. Earth Planet Sci Lett 181:327–340

Franz G, Andrehs G, Rhede D (1996) Crystal chemistry of monazite and xenotime from Saxthuringian–Moldanubian metapelites, NE Bavaria, Germany. Eur J Mineral 8:1097–1118

Gao S, Luo T-C, Zhang B-R, Zhang H-F, Han Y-W, Zhao, Z-D, Hu Y-K (1998) Chemical composition of the continental crust as revealed by studies in east China. Geochim Cosmochim Acta 62:1959–1975

Getty SR, Gromet LP (1992) Geochronological constraints on ductile deformation, crustal extension, and doming about a basement-cover boundary, New England Appalachians. Am J Sci 292:359–397

Gratz R, Heinrich W (1997) Monazite-xenotime thermobarometry: experimental calibration of the miscibility gap in the binary system $CePO_4$–YPO_4. Am Mineral 82:772–780

Gromet LP, Dymek RF, Haskin LA, Korotev RL (1984) The North-American shale composite—its compilation, major and trace-element characteristics. Geochim Cosmochim Acta 48:2469–2482

Grove M, Harrison TM (1999) Monazite Th–Pb age depth profiling. Geology 27:487–490

Hacker BR, Gnos E, Ratschbacher L, Grove M, McWilliams M, Sobolev SV, Wan J, Zhenhan W (2000) Hot and dry deep crustal xenoliths from Tibet. Science 287:2463–2466

Hanson LS, Bradley DC (1989) Sedimentary facies and tectonic interpretations of the lower Devonian Carrabassett Formation, north-central Maine. Maine Geol Surv Studies Maine Geol 2:101–125

Harrison TM, McKeegan KD, Le Fort P (1995) Detection of inherited monazite in the Manaslu leucogranite by $^{208}Pb/^{232}Th$ ion microprobe dating: crystallization age and tectonic significance. Earth Planet Sci Lett 133:271–282

Harrison TM, Ryerson FJ, Le Fort P, Yin A, Lovera OM, Catlos EJ (1997) A Late Miocene origin for the Central Himalayan inverted metamorphism. Earth Planet Sci Lett 146:E1–E7

Harrison TM, Grove M, McKeegan KD, Coath CD, Lovera OM, Le Fort P (1999) Origin and episodic emplacement of the Manaslu intrusive complex, central Himalaya. J Petrol 40:3–19

Harrison TM, Catlos EJ, Montel J-M (2002) U–Th–Pb dating of phosphate minerals. Rev Mineral Geochem 48:523–558

Hawkins DP, Bowring SA (1997) U–Pb systematics of monazite and xenotime: case studies from the Paleoproterozoic of the Grand Canyon, Arizona. Contrib Mineral Petrol 127:87–103

Heinrich W, Andrehs G, Franz G (1997) Monazite–xenotime miscibility gap thermometry. I. An empirical calibration. J Metamorph Geol 15:3-16

Hildebrand PR, Noble SR, Searle MP, Waters DJ, Parrish RR (2001) Old origin for an active mountain range: geology and geochronology of the eastern Hindu Kush, Pakistan. Geol Soc Am Bull 113:625–639

Holdaway MJ, Guidotti CV, Novak JM, Henry WE (1982) Polymetamorphism in medium- to high-grade pelitic metamorphic rocks, west-central Maine. Geol Soc Am Bull 93:572–584

Hueber FM, Bothner WA, Hatch NL Jr, Finney SC, Aleinikoff JN (1990) Devonian plants from southern Quebec and northern New Hampshire and the age of the Connecticut Valley trough. Am J Sci 290:360–395

Jasper J (2001) Quantitative estimates of precision for molecular isotopic measurements. Rapid Comm Mass Spectrom 15:1554–1557

Kingsbury JA, Miller CF, Wooden JL, Harrison TM (1993) Monazite paragenesis and U–Pb systematics in rocks of the eastern Mojave Desert, California, USA: implications for thermochronometry. Chem Geol 110:147–167

Kohn MJ, Catlos EJ, Ryerson FJ, Harrison TM (2001) P–T–t path discontinuity in the MCT zone, central Nepal. Geology 29:571–574

Kretz R (1983) Symbols for rock-forming minerals. Am Mineral 68:277–279

Krohe A, Wawrzenitz N (2000) Domainal variations of U–Pb monazite ages and Rb–Sr whole-rock dates in polymetamorphic paragneisses (KTB Drill Core, Germany): influence of strain and deformation mechanisms on isotope systems. J Metamorph Geol 18:271–291

Lanzirotti A, Hanson GN (1996) Geochronology and geochemistry of multiple generations of monazite from the Wepawaug schist, Connecticut, USA: implications for monazite stability in metamorphic rocks. Contrib Mineral Petrol 125:332–340

Lyons JB (1955) Geology of the Hanover quadrangle, New Hampshire-Vermont. Geol Soc Am Bull 66:105–146

Menard T, Spear FS (1993) Metamorphism of calcic pelitic schists, Strafford Dome, Vermont: compositional zoning and reaction history. J Petrol 34:977–1005

Menard T, Spear FS (1994) Metamorphic P–T paths from calcic pelitic schists from the Strafford Dome, Vermont, USA. J Metamorph Geol 12:811–826

Moore JM (1960) Phase relations in the contact aureole of the Onawa pluton, Maine. PhD Thesis, Massachusetts Institute of Technology

Novak JM, Holdaway MJ (1981) Metamorphic petrology, mineral equilibria, and polymetamorphism in the Augusta quadrangle, south-central Maine. Am Mineral 66:51–69

Osberg PH (1968) Stratigraphy, structural geology, and metamorphism of the Waterville–Vassalboro area, Maine. Maine Geol Surv Bull 20

Osberg PH (1979) Geologic relationships in south-central Maine. In: Skehan JW, Osberg PH (eds) The Caledonides in the USA: geological excursions in the northeast Appalachians. Boston College, Weston, Massachusetts, pp 37–62

Osberg PH (1988) Geologic relations within the shale-wacke sequence in south-central Maine. Maine Geol Surv Studies Maine Geol 1:51–73

Osberg PH, Hussey AM, Boone GM (1985) Bedrock geologic map of Maine. Maine Geological Survey, Augusta

Osberg PH, Tull JF, Robinson P, Hon R, Butler JR (1989) The Acadian orogen. In: Hatcher RD Jr, Thomas WA, Viele GW (eds) The Appalachian–Ouachita orogen in the United States. The geology of North America, vol F-2. Geological Society of America, Boulder, pp 179–232

Overstreet WC (1967) The geologic occurrence of monazite. US Geol Surv Prof Paper 530

Pan Y (1997) Zircon- and monazite-forming metamorphic reactions at Manitouwadge, Ontario. Can Mineral 35:105–118

Parrish RR (1990) U–Pb dating of monazite and its application to geological problems. Can J Earth Sci 27:1431–1450

Pattison DRM, Tracy RJ (1991) Phase equilibria and themobarometry of metapelites. Min Soc Am Rev Mineral 26:105–206

Philbrick SS (1936) The contact metamorphism of the Onawa pluton, Piscataquis County, Maine. Am J Sci 31:1–40

Plank T, Langmuir CH (1998) The chemical composition of subducting sediment and its consequence for the crust and mantle. Chem Geol 145:325–394

Pyle JM, Spear FS, Rudnick RL, McDonough WF (2001) Monazite–xenotime–garnet equilibrium in metapelites and a new monazite–garnet thermometer. J Petrol 42:2083–2107

Rasmussen B, Fletcher IR, McNaughton NJ (2001) Dating low-grade metamorphic events by SHRIMP U–Pb analysis of monazite in shales. Geology 29:963–966

Rasmussen B, Bengtson S, Fletcher IR, McNaughton NJ (2002) Discoidal impressions and trace-like fossils more than 1,200 million years old. Science 296:1112–1115

Rubatto D, Williams IS, Buick IS (2001) Zircon and monazite response to prograde metamorphism in the Reynolds Range, central Australia. Contrib Mineral Petrol 140:458–468

Sawka WN, Banfield JN, Chappell BW (1986) A weathering-related origin of widespread monazite in S-type granites. Geochim Cosmochim Acta 50:171–175

Shaw DM (1956) Geochemistry of pelitic rocks. Part III. Major elements and general geochemistry. Geol Soc Am Bull 67:919–934

Simpson RL, Parrish RR, Searle MP, Waters DJ (2000) Two episodes of monazite crystallization during metamorphism and crustal melting in the Everest region of the Nepalese Himalaya. Geology 28:403–406

Smith HA, Giletti BJ (1997) Lead diffusion in monazite. Geochim Cosomochim Acta 61:1047–1055

Smith HA, Barreiro B (1990) Monazite U–Pb dating of staurolite grade metamorphism in pelitic schists. Contrib Mineral Petrol 105:602–615

Spear FS, Harrison TM (1989) Geochronological studies in central New England I: evidence for pre-Acadian metamorphism in eastern Vermont. Geology 17:181–184

Spear FS, Parrish RR (1996) Petrology and cooling rates of the Valhalla complex, British Columbia, Canada. J Petrol 37:733–765

Stern RA, Berman RG (2000) Monazite U–Pb and Th–Pb geochronology by ion microprobe, with an application to in situ dating of an Archean metasedimentary rock. Chem Geol 172:113–130

Suzuki K, Adachi M (1994) Middle Precambrian detrital monazite and zircon from the Hida gneiss on Oki-Dogo Island, Japan: their origin and implications for the correlation of basement gneiss of southwest Japan and Korea. Tectonophysics 235:277–292

Suzuki K, Adachi M, Kajizuka I (1994) Electron microprobe observations of Pb diffusion in metamorphosed detrital monazites. Earth Planet Sci Lett 128:391–405

Symmes GH, Ferry JM (1995) Metamorphism, fluid flow and partial melting of pelitic rocks from the Onawa contact aureole, central Maine, USA. J Petrol 36:587–612

Thompson JB Jr (1957) The graphical analysis of mineral assemblages in pelitic schists. Am Mineral 42:842–858

Thompson JB Jr, Norton SA (1968) Paleozoic regional metamorphism in New England and adjacent areas. In: Zen E-A, White WS, Hadley JB, Thompson JB Jr (eds) Studies in Appalachian geology: northern and maritime. Interscience, New York, pp 319–327

Thompson JB Jr, Robinson P, Clifford TN, Trask NJ Jr (1968) Nappes and gneiss domes in west- central New England. In: Zen E-A, White WS, Hadley JB, Thompson JB Jr (eds) Studies in Appalachian geology. Northern and Maritime. Interscience, New York, pp 203–218

Townsend KJ, Miller CF, D'Andrea JL, Ayers JC, Harrison TM, Coath CD (2000) Low temperature replacement of monazite in the Ireteba granite, southern Nevada: geochronological implications. Chem Geol 172:95–112

Tucker RD, Osberg PH, Berry HN IV (2001) The geology of a part of Acadia and the nature of the Acadian orogeny across central and eastern Maine. Am J Sci 301:205–260

Vance D, Meier M, Oberli F (1998) The influence of high U–Th inclusions on the U–Th–Pb systematics of almandine-pyrope garnet: results of a combined bulk dissolution, stepwise-leaching, and SEM study. Geochim Cosmochim Acta 62:3527–3540